DOCTORAL DISSERTATION SERIES

PUBLICATION: 5031

AUTHOR: William Allen Doerner, Sc. D., 1952
University of Michigan

TITLE: DIFFUSION AND ADSORPTION OF HYDROGEN IN A POROUS NICKEL CATALYST

University Microfilms, Ann Arbor, Michigan, 1953

DIFFUSION AND ADSORPTION OF HYDROGEN IN A POROUS NICKEL CATALYST

By

William A. Doerner

A Dissertation Submitted in Partial Fulfillment of
the Requirements for the Degree of Doctor of Science
in the University of Michigan

1952

Committee in Charge:

Professor R. R. White, Chairman
Associate Professor J. T. Banchero
Professor F. E. Bartell
Associate Professor C. M. Sliepcevich
Professor Lars Thomassen

ABSTRACT

DIFFUSION AND ADSORPTION OF HYDROGEN IN A

POROUS NICKEL CATALYST

By

William A. Doerner

Adsorption isotherms and rates of adsorption on a nickel-kieselguhr catalyst were measured up to 30 atmospheres pressure in the temperature range 0°C to 300°C. The data were obtained with a volumetric adsorption apparatus designed and constructed for operation at pressures up to 30 atmospheres and temperatures from -196°C to 400°C. The apparatus consists essentially of a steel catalyst chamber and a glass gas burette both of which are thermostated. A mercury manometer is connected to the burette and a dead weight pressure gage tester is connected to the adsorbent chamber through a mercury leg. To minimize the effect of dead space the adsorbent chamber was scaled up to a volume of 250 cc.

An isotherm was calculated from the data obtained by the step-wise addition of hydrogen contained in the burette to the catalyst in the adsorbent chamber. Above one atmosphere pressure the data was obtained by the step-wise withdrawal of hydrogen from the adsorbent chamber. Equilibrium was re-established in each step of this process in about an hour at the higher pressures but below one atmosphere equilibrium was never attained even after waiting several days. It was found that the logarithm of the difference between the equilibrium pressure and the observed pressure was linear with time at long times. Therefore, in cases wherein equilibrium was not attained an equilibrium pressure was estimated and the estimate checked by this semi-logarithmic plot.

Above one atmosphere pressure the data gave straight lines when plotted according to the Langmuir equation. The equilibrium adsorption constant above one atmosphere pressure and at 200° and 300°C agrees with the constant obtained from catalytic hydrogenation studies

on the same catalyst. To obtain reproducible data it was necessary to reduce the catalyst 8 hours at 550°C using hydrogen at 30 atmospheres pressure and then to evacuate briefly at 400-500°C between runs.

The variation of the observed pressure during the first 10-30 minutes was found to be proportional to the square-root of time. Extrapolating to zero time gave an initial pressure whose magnitude indicated that adsorption was about 50 per cent complete instantaneously. This was interpreted to mean that the macropores of the catalyst were readily accessible and that diffusion and adsorption of hydrogen in the micropores accounted for the transient phenomena. From Langmuir's theory adsorption was estimated to be essentially instantaneous.

A differential equation representing one-dimensional diffusion in cylindrical pores accompanied by adsorption on the pore walls was solved for the case where the pores are bounded by a finite volume of gas. The solution was investigated using the slopes of the pressure-time data plotted according to the square-root of time at short times and the semi-logarithmic plot at long times. The results indicated that the micropores approached molecular dimensions and that the gas transport in the pores was of Knudsen type with a correction for the time-lag due to the average life of a molecule in the adsorbed state.

TO JOYCE

PREFACE

The original purpose of this investigation was the determination of the hydrogen equilibrium adsorption constant by an adsorption study for the comparison with the constant obtained in catalytic hydrogenation studies on the same catalyst. However, during the course of the investigation it was found that rates of adsorption could be readily measured so the scope of the problem was broadened to include a study of this rate process. This problem can be divided into the three following phases:

1. Developing and calibrating equipment suitable for measuring gas adsorption up to 30 atmospheres pressure and 400°C.

2. Developing a catalyst treatment and an operating procedure to obtain reproducible data.

3. Developing a theory to explain the adsorption rate process.

Valuable aid and advice in this work was provided by the writer's fellow graduate students and the members of his doctoral committee. In particular, the support of the Michigan Gas Association and the guidance of Professor R. R. White, chairman of the doctoral committee and supervisor of the Michigan Gas Association Fellowship, are gratefully acknowledged. The writer is also indebted to W. T. Boyd, Paul G. Davis, and J. A. Pursley for their help in the early phases of the work and to L. M. Naphtali for his aid in the final phases of this investigation.

TABLE OF CONTENTS

	Page
LIST OF TABLES	vi
LIST OF ILLUSTRATIONS	vii
LIST OF APPENDICES	viii
INTRODUCTION	1
APPARATUS	6
Adsorbent Chamber Unit	7
Water Bath Unit	11
Vacuum System	13
Gas Supply Panels	15
MATERIALS	18
Catalyst	18
Gases	18
EXPERIMENTAL PROCEDURE	19
Order of Operation	19
Catalyst Reduction and Evacuation	19
Isotherms	20
EXPERIMENTAL DATA	22
Operational Data	22
Equilibrium Pressure	24
Catalyst Pellet Description	26
EXPERIMENTAL AND THEORETICAL RESULTS	28
Langmuir Isotherm	28
Catalyst Area	30
Equilibrium Adsorption Constant	30
Rate of Adsorption	30
Short-Time Data	33
Readily Accessible Surface	36
High-Pressure Catalyst Reduction	36
Diffusion in Catalyst Pores	38
Comparison of B Values	47
Diffusivity	49
Micropore Size	51
Effusion in Catalyst Pores	52
Diffusion of Helium	54

TABLE OF CONTENTS (cont)

	Page
DISCUSSION	[illegible]
Apparatus	[illegible]
Results	[illegible]
CONCLUSIONS	[illegible]
APPENDICES	[illegible]
BIBLIOGRAPHY	[illegible]
NOMENCLATURE	[illegible]

LIST OF TABLES

Table		Page
1.	Description of an Average Cylindrical Catalyst Pellet	27
2.	Comparison of Values of B Calculated by Different Methods	49
3.	Iron-Constantan Thermocouple Calibration	65
4.	Compressibility of Hydrogen and Helium	66
5.	Calibration of the Burette Volume	68
6.	Summary of Volume Calibration	68
7.	Catalyst Free Space Corrections	69
8.	Catalyst Free Space	69
9.	Experimental Pressure-Time Data	71
10.	Data Summary	76
11.	Sample Calculations. Run 18 (0°C)	82
12.	Summary of Sample Calculations. Run 18 (0°C)	82
13.	Hydrogen Adsorption Isotherms on Nickel-Kieselguhr	84
14.	Fraction of Catalyst Surface Readily Accessible	85
15.	Calculation of V_pD/L^2 from Initial Slopes	86
16.	Calculation of V_pD/L^2 from Final Slopes	87
17.	Summary of V_pD/L^2 Calculations	88
18.	Sources of Equipment and Materials	110

LIST OF ILLUSTRATIONS

Figure		Page
1.	Volumetric Adsorption Equipment.....	8
2.	Schematic Diagram of Equipment.....	9
3.	Schematic Diagram of Electrical Units.....	10
4.	Adsorbent Chamber and Jacket.....	12
5.	Schematic Diagram of Gas Supply Panel.....	17
6.	Hydrogen Adsorption Isotherms on Nickel-Kieselguhr.....	43
7.	Determination of the Equilibrium Pressure.....	45
8.	Hydrogen Adsorption Isotherms Plotted According to the Langmuir Equation.....	49
9.	Determination of Initial Pressure.....	55
10.	Fraction of the Catalyst Surface Readily Accessible.....	57
11.	Variation of V_pD/WL^2 with Pressure.....	46
12.	Water Bath Thermometer Calibration Curve.....	63
13.	Iron-Constantan Thermocouple Calibration Curve.....	64
14.	Solutions of the Equation $\beta \cot \beta + B = 0$.....	100
15.	Micropore Consisting of a Series of Connecting Chambers.....	105
16.	Tuning Eye Contact Indicator.....	112

LIST OF APPENDICES

Appendix		Page
I.	CALIBRATION OF EQUIPMENT.....	62
	Temperature	62
	Water Bath Thermometer	62
	Thermocouple	62
	Pressure	65
	Manometer	65
	Dead Weight Tester	66
	Compressibility	66
	Volume	67
	Burette	67
	Secondary Volumes	67
	Catalyst Free Space	69
II.	EXPERIMENTAL DATA.....	70
	Experimental Pressure-Time Data	71
	Data Summary	76
III.	DATA PROCESSING.....	80
	Isotherms	81
	Sample Calculations. Run 18 (0°C.)	82
	Summary of Sample Calculations. Run 18 (0°C.)	82
	Hydrogen Adsorption Isotherms on Nickel-Kieselguhr	84
	Fraction of Catalyst Surface Readily Accessible	85
	Diffusion	83
	Calculation of V_pD/L^2 from Initial Slopes	86
	Calculation of V_pD/L^2 from Final Slopes	87
	Summary of V_pD/L^2 Calculations	88
IV.	DERIVATIONS.....	89
	The Langmuir Adsorption Isotherm	90
	The Rate of Adsorption at Constant Volume	93
	Diffusion and Adsorption in Cylindrical Catalyst Pores	97
	Effusion and Adsorption in a Porous Catalyst	105

LIST OF APPENDICES (cont)

Appendix		Page
V.	NOTES ON EQUIPMENT.....	109
	Sources of Equipment and Materials	110
	Tuning Eye Contact Indicator	111

DIFFUSION AND ADSORPTION OF HYDROGEN IN A POROUS NICKEL CATALYST

The adhesion of the molecules of a gas to the surface of a solid with which the gas is in contact is known as adsorption. There are two types of adsorption, one referred to as van der Waals or physical adsorption and the other as activated adsorption or chemisorption. In van der Waals adsorption there is weak interaction between gas and solid and the energy change accompanying this type of adsorption is of the same order as the heat of condensation. Chemisorption, on the other hand, involves large energy changes such as occur in chemical reactions. It is a highly specific phenomena and is generally assumed to occur on certain active centers which may represent only a small fraction of the total surface (Taylor, 1A). While both activated and physical adsorption may be encountered at the same temperature, above the critical temperature of the adsorbate adsorption is almost entirely of the activated type (10). It is with this type of adsorption that the present investigation will be concerned.

When a reaction is catalyzed by a solid it is assumed that one or more of the reactants is adsorbed on active centers on the catalyst surface. The reaction mechanism, therefore, involves adsorption of reactants, surface reaction, and desorption of products. Complete reaction rate equations based on these three steps are too complex to be of any practical value. Therefore, it is usually satisfactory to assume that the rate is

controlled by a single slow step and that all other steps are so fast that equilibrium may be assumed. Hougen and Watson (17, chapter XIX) show the method of deriving rate equations based on the various possible rate-controlling mechanisms. These equations always contain one or more equilibrium adsorption constants which are defined as the ratio of the concentration of an adsorbed component to the product of the concentration of the vacant active centers and the equilibrium pressure of that component. In correlating reaction rate data it is customary to select the rate equation that fits the data best over the range of variables studied. The only restriction imposed on the rate equation constants in this data-fitting process is that they be positive. Therefore it would seem to be advantageous to determine the magnitude of the equilibrium adsorption constants by independent adsorption studies. However, Hougen stated in the discussion which followed the presentation of Potter and Baron's (27) paper on kinetics that it seems doubtful that "equilibrium adsorption constants obtained in separate adsorption experiments with the separate gases should be used in the rate equation for the catalytic reaction." He argued that a catalytic reaction is concerned with a few special active centers on the catalyst in a narrow concentration range while an adsorption experiment is concerned with the entire catalyst surface. Furthermore, the equilibrium adsorption constant varies widely with concentration. Schwab (1B) agreed with Hougen and gave a similar reason. This presents an interesting situation which would appear to warrant further attention. The present investigation was undertaken to determine the hydrogen equilibrium adsorption constant and compare it with the constant obtained in the catalytic hydrogenation studies by Pursley (28) and Binder (9) on the same catalyst.

To obtain data in the same region that Pursley and Binder studied it was necessary to build equipment capable of operation up to 400°C. and 30 atmospheres pressure. The apparatus, which was designed to measure gas adsorption by the volumetric method, consists essentially of an adsorbent chamber and a gas burette. Both are thermostated and have pressure indicating devices. In the volumetric method the amount of gas adsorbed is determined as the difference between the gas initially in the adsorbent chamber, the burette, and the connecting manifold and the gas in these spaces after a quantity of gas from the burette has been admitted to the adsorbent. Above one atmosphere pressure gas is desorbed from the adsorbent by drawing off successive quantities of gas into the burette.

One unexpected result of the experimental work of this investigation was that several hours were usually required for the pressure to reach equilibrium whenever a quantity of hydrogen was admitted to or withdrawn from the adsorbent chamber. This length of time facilitated measurement of the rate of adsorption to such an extent that the scope of the investigation was broadened to include a study of this rate process. Rates of adsorption have been attributed to solution, migration, surface reaction, activated adsorption, and diffusion into the fine pores of the adsorbent. The last process proved to be the best explanation for the results of this investigation.

By studying the diffusion rate it should be possible to learn something of the pore structure which is of considerable interest in catalysis. Wheeler (1C) states that "two catalysts, chemically identical, but having pores of different size, may have different activities, different selectivities, different temperature coefficients of reaction rate, and catalyst poisons may affect the two catalysts in quite different ways." To allow for

the effect of diffusion in catalyst pores on rate of reaction, Thiele (33) developed a correction factor which is a function of a certain modulus. This modulus depends upon the average pore length and diameter, the diffusion coefficient, and the reaction velocity constant. Since these factors are usually not all known Hougen and Watson (17, p. 995) developed a modification of Thiele's theory which does not require such precise information.

Many techniques exist for studying a catalyst pore structure. Barrett et al. (7) present a method for determining the pore volume and area distribution from low-temperature nitrogen adsorption isotherms which is suitable for measuring small pores while Ritter and Drake (29) have developed a high-pressure mercury porosimeter method suitable for large-pore measurements. Joyner et al. (19) found that both of these procedures agree well in the region they overlap. Further methods and summaries of earlier literature appear in Advances in Catalysis (1A, 1B, and 1C) and Brunauer (10).

An interesting technique was recently used by Barrer and Grove (6). They allowed gas to flow through a column of porous crystals and from the time-lag in setting up the steady state of flow, they calculated the mean pore radius, the internal surface, and the diffusivity. Since this procedure measures the same portion of the catalyst in which reactions probably take place it should be especially well suited to calculating the Thiele modulus.

In summary, the present investigation may be divided into three phases: (1) a determination of the equilibrium adsorption constant, (2) an attempt to show that the adsorption rate process is due to diffusion of hydrogen into the fine pores of the catalyst, and (3) a study of the

diffusion rate in order to obtain information on the catalyst pore structure. The theoretical part of this investigation is more easily understood if the apparatus and experimental data are examined first. Therefore the discussion of the experimental and theoretical results will be postponed until after the equipment and experimental data have been considered in some detail.

APPARATUS

The apparatus consists of an adsorbent chamber in which the adsorbent is placed, a gas measurement system, and auxiliary equipment which includes a gas supply system and a system for evacuating the adsorbent. The amount of gas adsorbed by the adsorbent is determined as the difference between the gas initially in the adsorbent chamber, the burette, and the connecting manifold and the gas in these spaces after a quantity of gas from the burette has been admitted to the adsorbent. The amount of gas in each of these spaces is calculated from pressure, temperature, and volume measurements.

The apparatus was designed to obtain adsorption data by the volumetric method in a pressure range from one millimeter to 30 atmospheres and from liquid nitrogen temperatures to 400°C. The size of the equipment was determined by considering its effect on a desorption run. In a desorption run the amount of gas desorbed is the difference between the amount of gas in the manifold and the free space in the adsorbent chamber initially, and the sum of the amount of gas in the free space finally and the amount of gas withdrawn into the burette. When operating at high pressure the catalyst free space and the dead space in the manifold between the burette and the adsorbent chamber contain large quantities of gas compared to the amounts being desorbed. This means that the amount of gas desorbed must be calculated by taking the difference of two large numbers. In order to minimize the effect of the dead space the adsorbent chamber volume was scaled up by a factor of about one hundred over the conventional chamber size.

The general layout of control panels, equipment rack, gas cylinders, service lines, piping, and electrical terminal box is the same as was used by Pursley (28) for his catalytic testing unit. One difference is the addition of a constant-temperature water bath between the control panels and the equipment rack. The equipment consists functionally of four major units: an adsorbent chamber unit, a water bath unit, a vacuum system, and the gas supply panels. These units are described in the following paragraphs and their interrelation is shown in Figs. 1-3.

The gas lines connecting the equipment were made of 20 gauge, 52S-O aluminum tubing except the steel tubing used in the water bath. The equipment sources are listed in Table 18 of Appendix V.

Adsorbent Chamber Unit

The adsorbent chamber and its constant-temperature bath shown in Fig. 4 constitute the adsorbent chamber unit. Constant temperature is obtained by refluxing a boiling liquid in a pressurized jacket surrounding the adsorbent chamber.

The adsorbent chamber consists of a 5-inch length of 2-inch ips. schedule 80 stainless-steel tubing with welded ends. The inlet head is machined to take an Aminco (American Instrument Company) 1/4-inch union-type superpressure connection. A short piece of tubing welded to the inlet head conducts the gas to the center of the adsorbent chamber. The bottom piece has a 3/4-inch hole for filling and is sealed with a plug flange machined with a 58°-60° cone closure and bolted with eight 3/8-inch 16 cap screws.

The adsorbent chamber heating jacket was fabricated from an 11-inch length of 5-inch ips. seamless steel pipe, a 300-lb. slip on flange, and

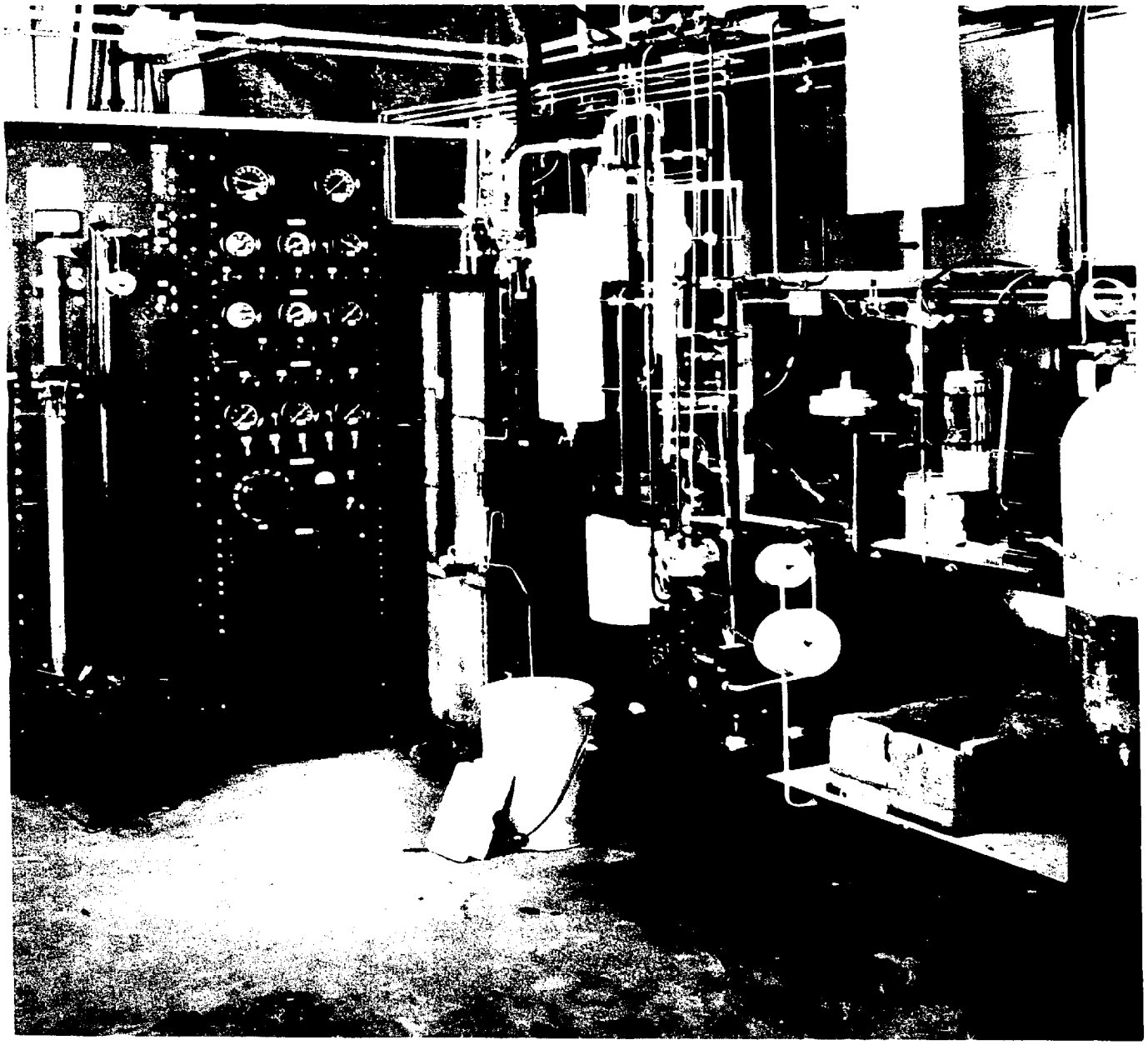

FIG. I VOLUMETRIC ADSORPTION EQUIPMENT

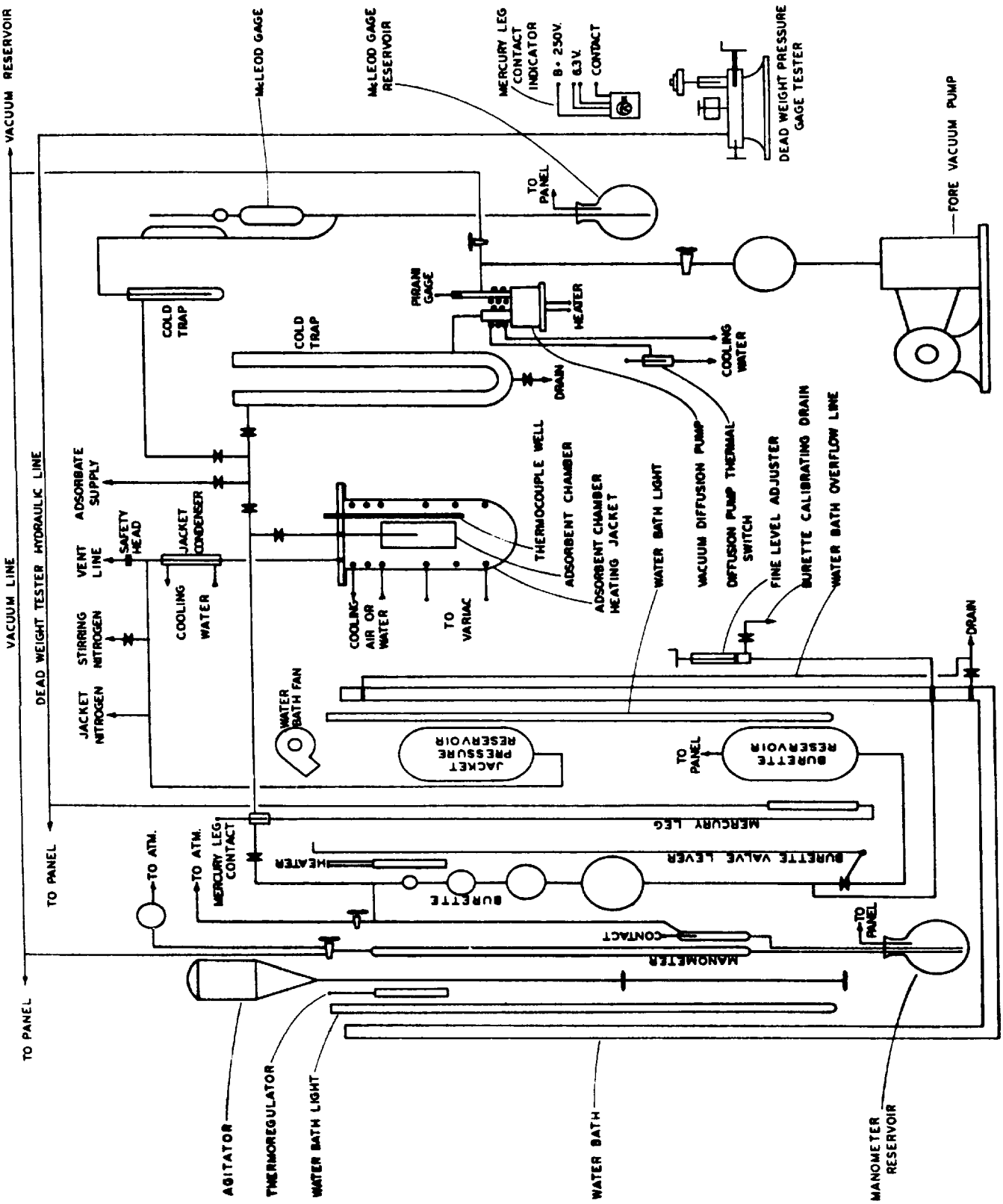

FIG. 2 SCHEMATIC DIAGRAM OF EQUIPMENT

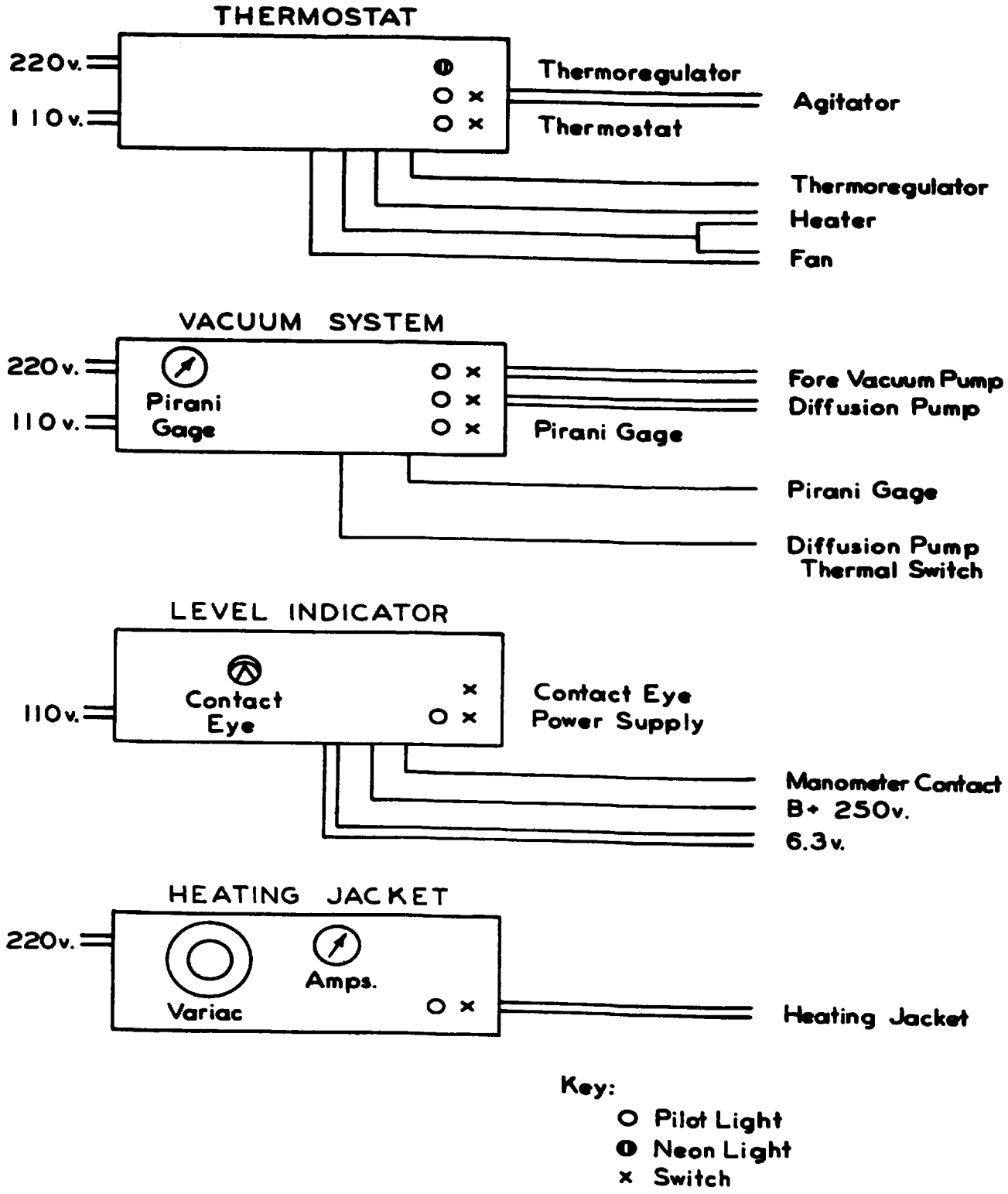

FIG. 3 SCHEMATIC DIAGRAM OF ELECTRICAL UNITS

a welding cap. The jacket bolts to a 300-lb. blind flange which is mounted permanently on the equipment rack. A 2500-w. 230-v. calrod heater in the bottom of the jacket boils the water or Dowtherm in the jacket which is then condensed by the water-cooled condenser mounted in the top of the blind flange. The power for the heating coil is supplied by an autotransformer shown in Fig. 3. The boiling point of the liquid used is controlled by pressurizing the jacket system with nitrogen. Since steady temperatures require constant nitrogen pressure a reservoir was placed in the water bath and connected to the top of the jacket condenser. This additional volume minimizes the temperature drift due to nitrogen leakage from the system. A 245-psi. rupture disc located at the top of the condenser protects the system. The jacket is insulated with 2 inches of 85 per cent magnesia and the flanges by a 2-inch thick Foamglas box. Temperature measurement is provided by an iron-constantan thermocouple and a K2 potentiometer. The thermocouple wires are shielded by a 1/4-inch steel tube.

Copper cooling coils are located near the top of the jacket to facilitate its removal. High temperatures are obtained by replacing the jacket with an electrical resistance furnace which is controlled with the jacket heater autotransformer. For low-temperature work a 4-qt. Dewar flask is placed around the adsorbent chamber. Liquid nitrogen can be stirred by connecting a tube to the bottom of the condenser pipe and cracking the needle valve on the nitrogen stirring line.

Water Bath Unit

The purpose of the water bath is to maintain a constant temperature of 25°C. for the gas measuring burette and the mercury manometer. An I-beam

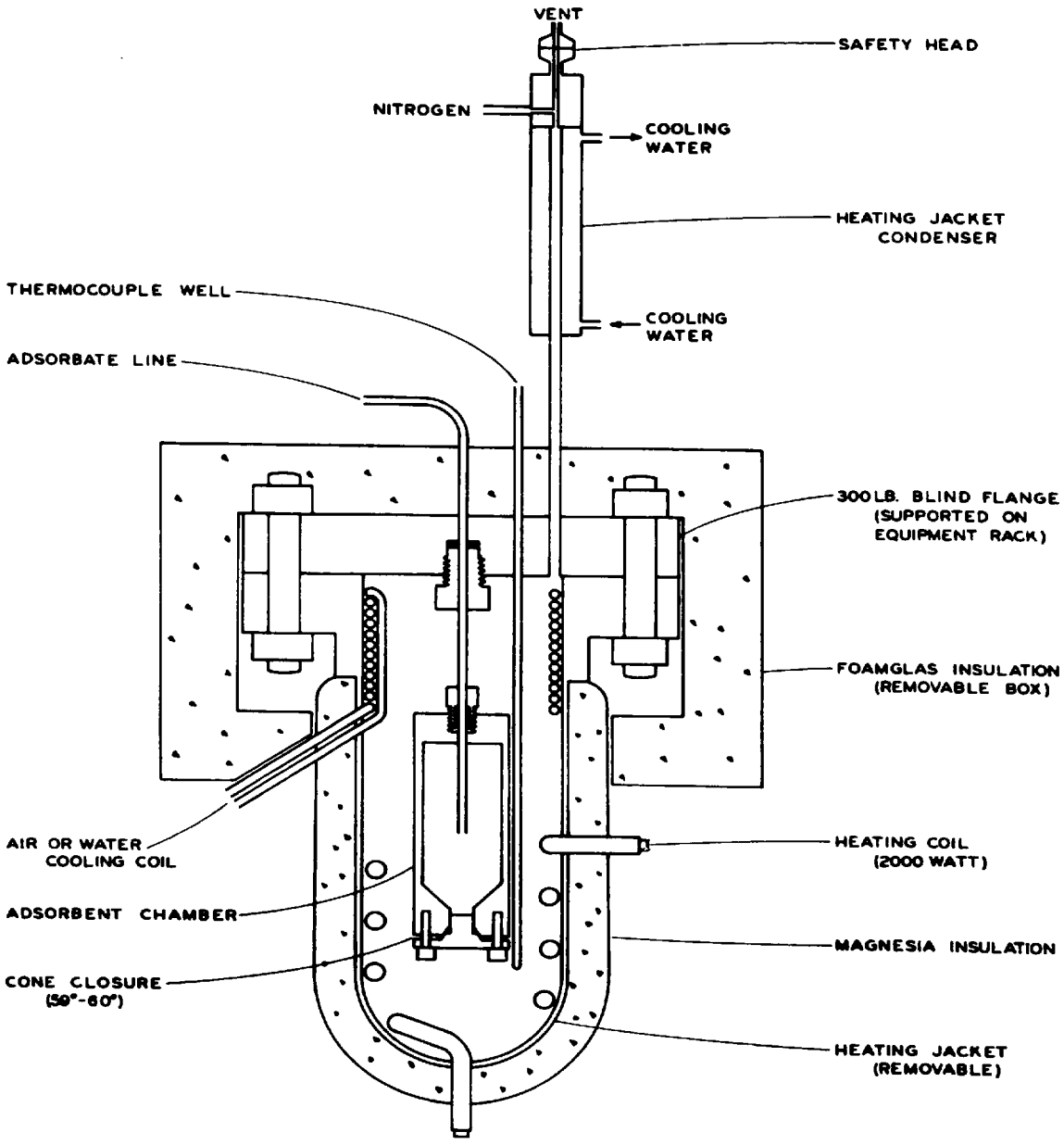

FIG. 4 ADSORBENT CHAMBER AND JACKET

suspended vertically from the equipment rack provides support for the equipment located in the bath. The water bath is constructed of sheet steel welded to an angle iron frame and insulated with 2 inches of Foamglas. Its inside dimensions are 13" x 15" x 55". The front side is removable and is gasketed with a 2" x 1/4" strip of foam rubber. A 1/2" x 3" x 33" Lucite window is located in the front side and the bath is illuminated by two 42-inch Slimline fluorescent lamps placed in glass tubes. Agitation is provided by a 1/4-horsepower portable power mixer with a 5-foot shaft and two 3-inch propellers.

Constant temperature is maintained by a vacuum-tube relay developed by Sucher and Anker (32) which operates in conjunction with an electric heater and an air blower. The thermostat is actuated by a toluene thermoregulator described by Snyder and Seltz (31) which was modified by using a Kovar-glass seal. Additional cooling in hot weather was obtained by installing a water bath overflow pipe and then directing a stream of cold water into the bath. Corrosion was kept to a minimum if this stream of water and the agitator were kept running continuously and if a few grams of potassium dichromate were added to the water bath daily. In addition a coating of tar was applied to all steel tubing in the water bath.

Four glass bulbs in series make up the gas measuring burette. A steel reservoir holds the mercury which is forced into the burette with nitrogen pressure. When the mercury reaches approximately the desired scribe mark between two burette bulbs, the burette toggle valve is closed by means of the valve lever and the mercury is leveled precisely with the

fine level-adjusting screw. The glass tube from the top of the burette is sealed with De Khotinsky cement to the steel tube leading to the adsorbent chamber.

The mercury manometer consists of two parallel one-inch I.D. glass tubes which lead separately into a mercury reservoir (Barr and Anhorn, 3). A 2-mm. bore glass capillary tube connects the short manometer leg to the top of the burette. The mercury level in this short leg is kept fixed at the tip of a tungsten pointer which is indicated by the tuning eye (Appendix V) shown in Fig. 3. Both legs are read through the water bath window with a cathetometer. The long leg may be operated at atmospheric pressure or under vacuum.

High pressure in the adsorbent chamber is indicated by a gage on the gas supply panel but is measured precisely with a dead weight pressure gage tester. These devices are connected by oil-filled lines to a mercury leg which transmits pressure to the oil from the gas in the manifold between the adsorbent chamber and the burette. It is necessary that the height of the mercury leg be kept fixed so that its pressure contribution and the manifold volume are constant. This is achieved by placing a contact at the top of the mercury leg which operates a tuning eye (Appendix V) located next to the dead weight tester. The mercury level is adjusted by turning the dead weight tester displacement screw. This arrangement proved to be so sensitive that in addition to the 1- and 2-lb. weights specially provided by the manufacturer it was necessary to make up weights down to 0.1 lb. To make the mercury contact a 1" x 2" x 2" block of steel was drilled in the form of a cross and one hole threaded to take an Aminco

superpressure electrical connector. The soapstone cone in the connector was replaced with a Teflon cone. The manifold and mercury leg steel tubes were welded into the other three holes in the contact fitting.

Vacuum System

The vacuum system is used to clean the adsorbent surface of adsorbed impurities before starting a run. In addition the vacuum maintained in the fore vacuum reservoir is used to manipulate the mercury levels in the various mercury reservoirs.

The vacuum system consists of a fore pump, Pirani gage, diffusion pump and cold trap, McLeod gage and cold trap, and fore vacuum reservoir (No. 1A gas cylinder). When the adsorbent chamber is operated at high pressure the vacuum system is isolated by means of two Hoke bellows valves which will take 500 psi. under their seats. The glass McLeod gage and cold trap are joined to the one-inch pipe from the bellows valve by a standard taper joint sealed with De Khotinsky cement.

A DPI type VMF-2W diffusion pump is operated with silicone pump oil DC703. To protect the pump and vacuum system, a thermal switch was placed in the exit cooling water line of the diffusion pump. This switch operates a relay which turns off the diffusion pump heater if the cooling water fails.

The Pirani gage is used as a leak and forevacuum detector. It was built according to the specifications of Schwartz and Lavender (30).

Gas Supply Panels

The gas supply panels shown in Fig. 5 service the rest of the equipment. The adsorbate and nitrogen panels reduce the cylinder gas pressure through Grove regulators to the desired pressure. Vacuum or nitrogen at any desired pressure can be connected to any mercury reservoir in the equipment

through the operating manifold. For fine adjustments of mercury reservoir levels, a small gas cylinder (manifold reservoir) is connected to the operating manifold. This panel also provides the nitrogen for pressurizing the adsorbent chamber. Hoke toggle valves and needle valves are used in the gas supply system, the latter being used wherever it is necessary to throttle the gas flow.

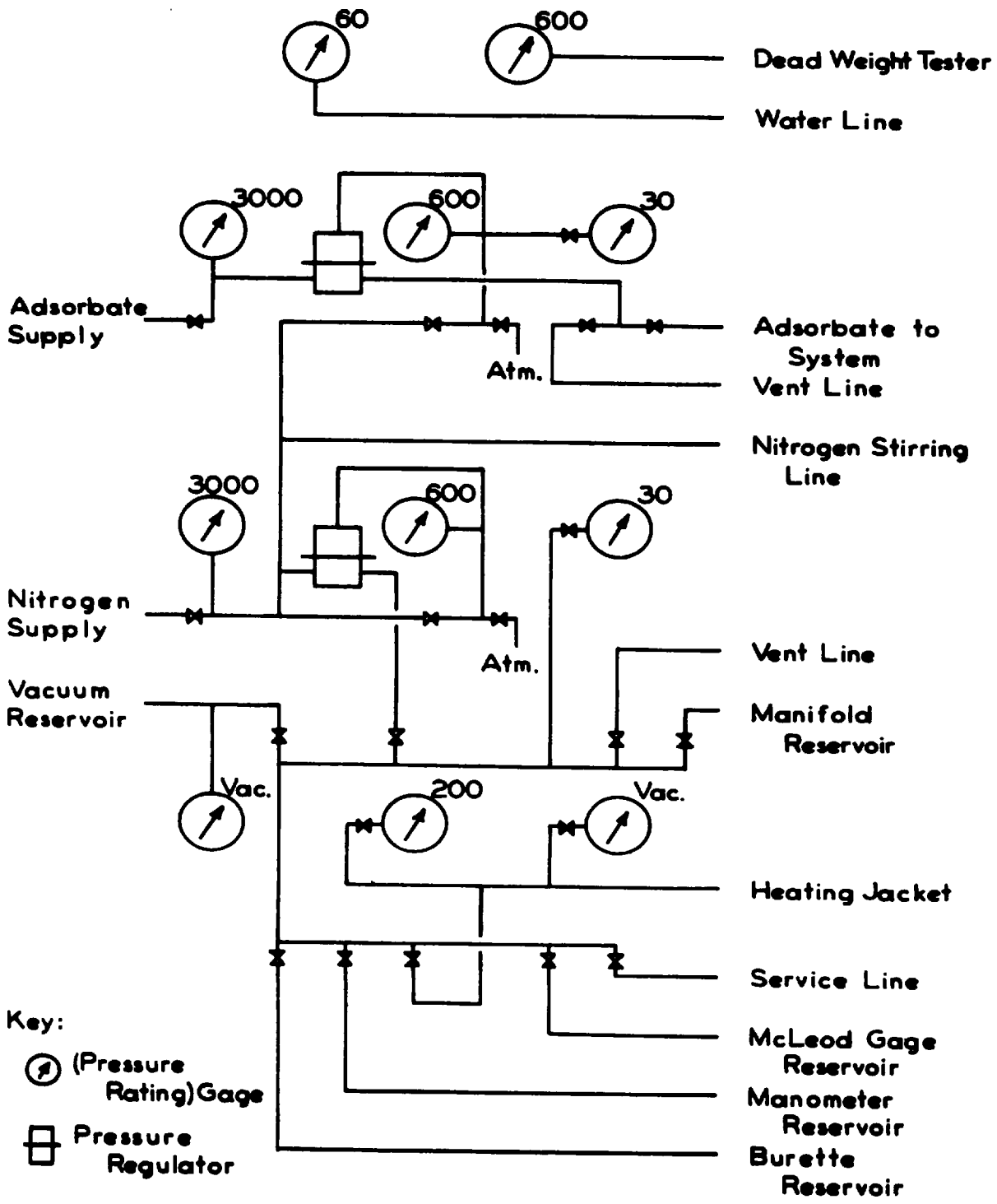

FIG. 5 SCHEMATIC DIAGRAM OF GAS SUPPLY PANEL

MATERIALS

The following paragraphs present a description of the catalyst and an analysis of the gases used. Table 1 in the section on experimental results gives additional information about the catalyst. A list of materials used in the construction and operation of the equipment may be found in Table 18 of Appendix V.

Catalyst

The catalyst was supplied by the Harshaw Chemical Company and is designated as Reduced Nickel 88 (Lot No. 219-1-14). It is the same type of nickel-kieselguhr catalyst used by Pursley (28), Binder (9), and Akers (2) in their kinetic hydrogenation studies. The catalyst reduction is described in the section on experimental procedure.

Gases

Electrolytic hydrogen was supplied by the Matheson Company and contains less than 0.2 per cent water (25). The helium (Matheson Company) used for the free space measurements is over 99.8 percent pure. The impurity is nitrogen with a small amount of hydrogen. For operating the equipment, nitrogen supplied by the Bird Company was used.

EXPERIMENTAL PROCEDURE

This section is divided into discussions of the order of operation, catalyst reduction, and procedure for obtaining an isotherm. The term "run" will be used here synonymously with isotherm. A run, therefore, includes the data obtained at one temperature in one consecutive series of steps which always start with an evacuated adsorbent. The calibration of the equipment is presented in Appendix I.

Order of Operation

The catalyst was first reduced with hydrogen at low pressure, evacuated, and hydrogen isotherms at 0°C., 100°C., 200°C., and 300°C. obtained. Check runs at 0°C. made after the completion of each isotherm indicated that initial reduction was not sufficient so the catalyst was further reduced with high-pressure hydrogen just prior to the 200°C. isotherm. The helium free space of the adsorbent chamber was determined initially and at the conclusion of the runs. Between runs the catalyst was always flushed several times with either hydrogen or helium depending upon which gas was to be used next and then evacuated at high temperature.

Catalyst Reduction and Evacuation

Before using a catalyst it is necessary to reduce it and free it as completely as possible from previously adsorbed gases. The purification is accomplished by evacuation at high temperature. Since sintering of the catalyst takes place at high temperatures it is necessary to compromise between the amount of sintering that can be tolerated and the degree of surface purity desired.

The high temperature (400°C.-550°C.) for reduction and evacuation was obtained by installing an electric furnace around the adsorbent chamber. During the reduction period the catalyst was repeatedly flushed with hydrogen followed by rough evacuation. The catalyst was cleaned before each run by heating under vacuum to 400°C. and immediately cooling the furnace. Then the furnace was removed, the catalyst brought to the temperature of the next run, and the evacuation continued overnight.

Isotherms

The data for one isotherm consist of an adsorption portion and a desorption portion. Starting with the evacuated catalyst a quantity of gas in the burette is allowed to equilibrate with the catalyst. Successive measured quantities of gas are admitted to the catalyst until the equilibrium pressure approaches one atmosphere. Then 450 to 500 psig. of gas is charged into the adsorbent chamber and several hours allowed for equilibration. A quantity of gas is drawn off in the burette and time is allowed for equilibrium to be re-established. Successive measured quantities of gas are removed in this manner until the final desorption equilibrium pressure is below the final adsorption equilibrium pressure. This overlapping permits data from both portions of the run to be fitted together. In the last step in the desorption portion of a run (when the final pressure is below one atmoshpere) the valves between the adsorbent chamber and the burette section are left open and the approach to equilibrium pressure is followed on the manometer rather than the dead weight tester.

In addition to the PVT data obtained in a run as described above it is necessary to have one more fact before the quantities of gas adsorbed or desorbed can be computed. That is the dead space or free space in the

adsorbent chamber surrounding the catalyst and including the pore space within the catalyst itself. This volume is measured in the manner described in Appendix I using helium with the adsorbent chamber at 0°C. The adsorption of helium at 0°C. is considered negligible (10, p. 33).

A special run was carried out at 0°C. by allowing helium at 500 psig. to equilibrate with the catalyst and then suddenly venting the adsorbent chamber. With the burette volume set at zero the vent was immediately closed and the pressure rise followed on the manometer.

EXPERIMENTAL DATA

This section is divided into discussions of the operational data, the method of determining the equilibrium pressure, and a description of the catalyst pellet. The isotherm data are presented in Tables 9 and 10 of Appendix II and the method of calculating the adsorption isotherms from this data is shown in Appendix III. Fig. 6 of this section presents the hydrogen adsorption isotherms based on the information in Table 13 of Appendix III.

Operational Data

The adsorbent chamber was filled with 370.39 grams of catalyst and the catalyst was reduced for 8 hours at 550°C. During this period the catalyst was flushed several times with hydrogen at 35 psig. followed by rough evacuation. Then the catalyst was cooled and evacuated overnight. The next morning the adsorbent chamber pressure was 3×10^{-4} mm. and it rose to 4×10^{-4} mm. with the vacuum system shut off for 10 minutes.

Check Run 15 at 0°C. shown in Fig. 6 followed the 100°C. isotherm and gave a marked increase in adsorption over the 0°C. isotherm. Apparently some reduction took place at the high-pressure end of the 100°C. isotherm. Therefore the catalyst was further reduced at 400°C. for one hour with 550 psig. hydrogen. Check Runs 18 and 20 at 0°C. indicate that the catalyst was stable beyond Run 15. The data for the 0°C. and 100°C. isotherms which were obtained before the catalyst was completely reduced were not included with the experimental data listed in Appendix II.

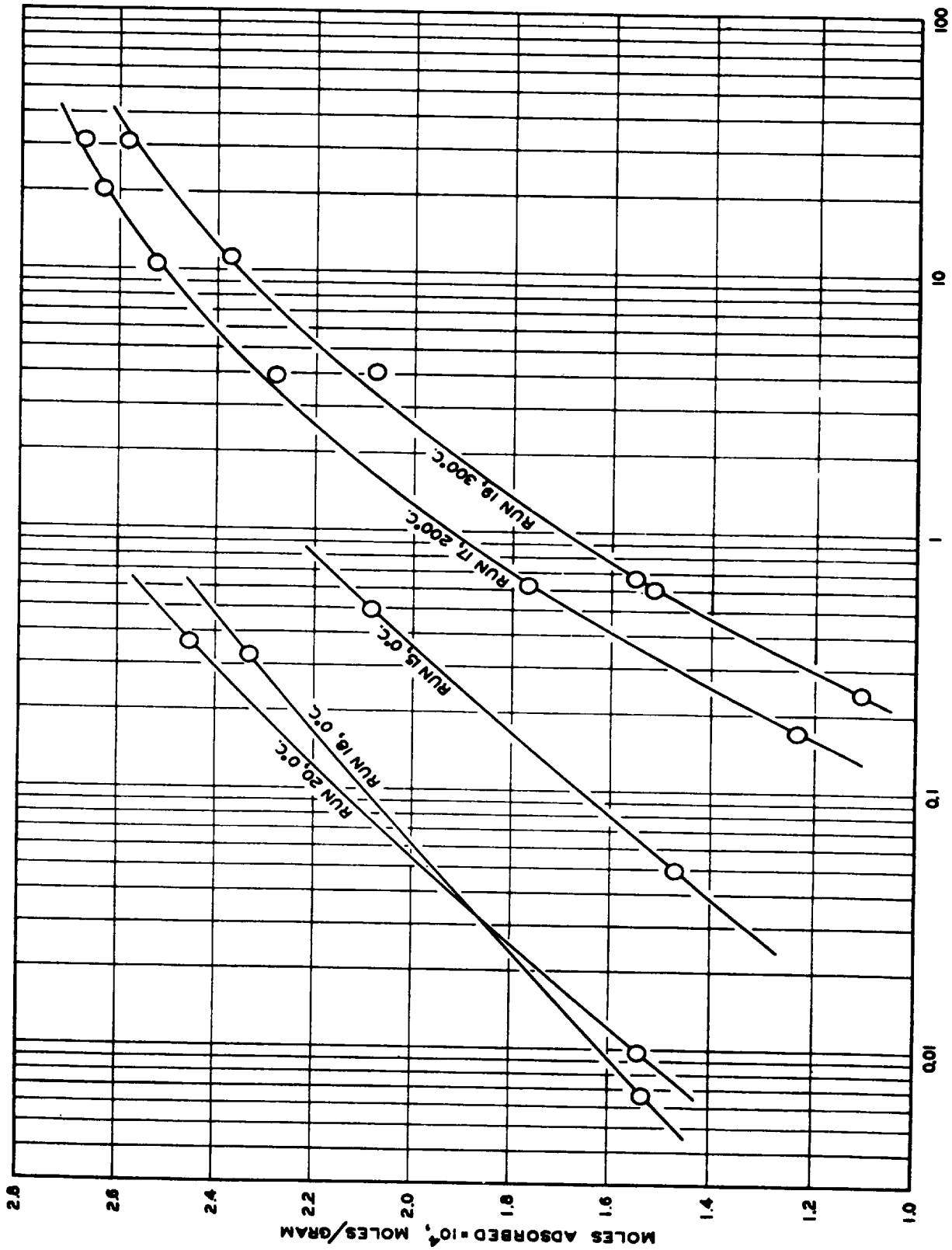

FIG. 6 HYDROGEN ADSORPTION ISOTHERMS ON NICKEL-KIESELGUHR

Run 17 (200°C.) was made using Dowtherm E in the catalyst chamber jacket and Run 19 (300°C.) using Dowtherm A. During these runs the temperature rarely fluctuated more than 0.1°C. Between runs the catalyst was heated under vacuum to 400°C., cooled, and evacuation continued overnight. A pressure of 10^{-3} mm. was usually obtained.

Equilibrium Pressure

Each time a quantity of gas was added to or withdrawn from the catalyst chamber a length of time was allowed for equilibrium to be re-established. Although equilibrium was reached (with respect to the sensitivity of the apparatus) at the higher pressures in about an hour, at pressures below one atmosphere equilibrium was never attained. In the data included here upwards to 24 hours were allowed between steps although at one time pressure changes were still observed at the end of 5 days.

If p is the pressure at time θ and p_∞ is the equilibrium pressure then it is found that a plot of $\ln (p_\infty - p)$ versus time gives a straight line except for the data at initial times. For cases where p_∞ is approached but not reached it is possible to estimate a value of p_∞ and plot $\ln (p_\infty - p)$ versus time as before. Fig. 7 is an example of such a case. If the estimate of p_∞ is too high or too low a straight line is not obtained so that by trial and error it is possible to find a value of p_∞ which will give a straight line at least through the last three points. All of the values of p_∞ listed in Table 10 of Appendix II which were not measured directly were obtained from the data in Table 9 using this trial and error procedure. Since the pressure decreases during an adsorption step and increases during a desorption step it is necessary to plot $\ln (p - p_\infty)$ for an adsorption step instead of $\ln (p_\infty - p)$.

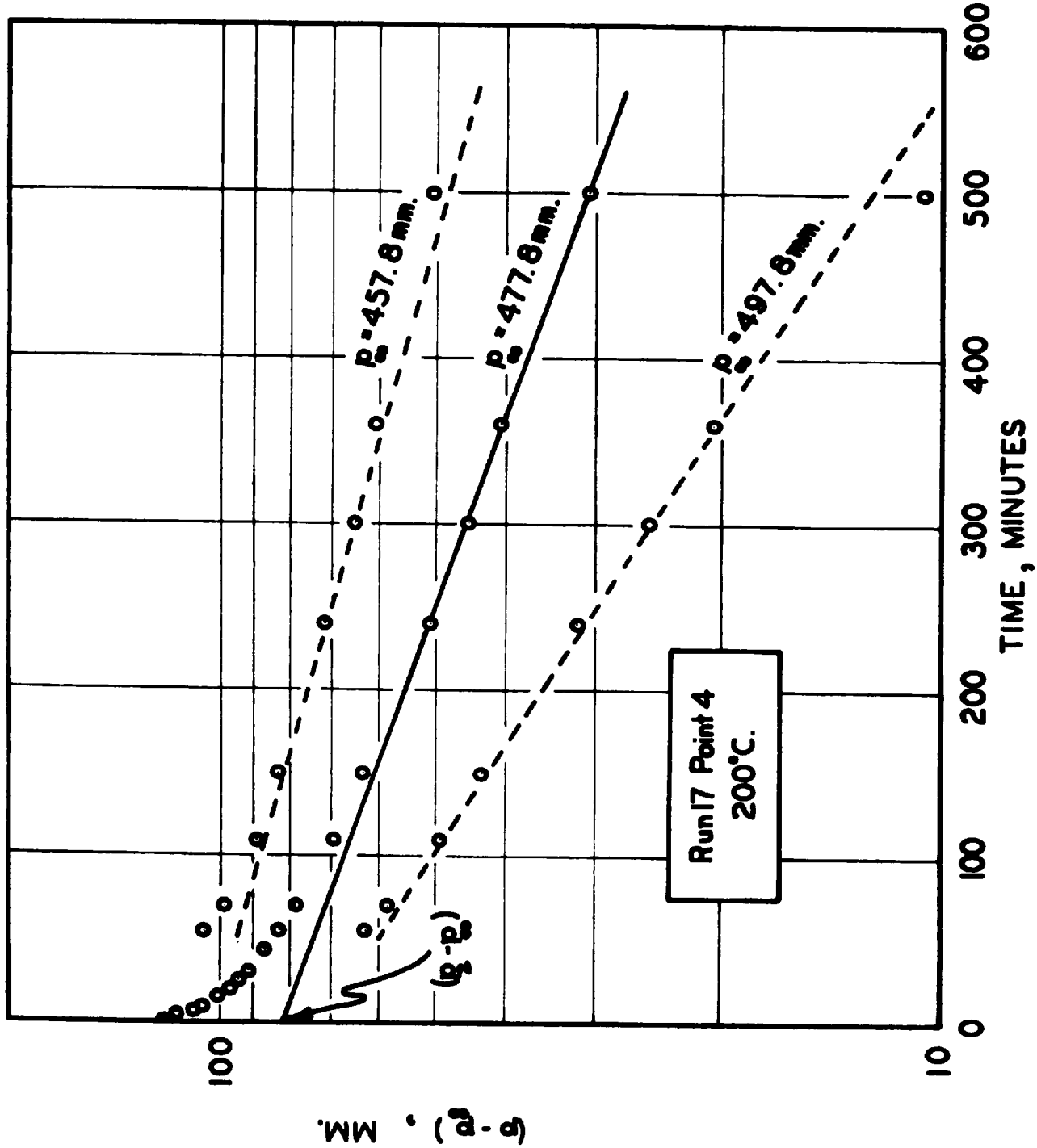

FIG. 7 DETERMINATION OF THE EQUILIBRIUM PRESSURE

A check on the 200°C. and 300°C. isotherms revealed that adsorption or desorption was at least 97 per cent complete at the final pressure experimentally attained in each step with three exceptions. In Points 4 and 10 of Run 17 and Point 4 of Run 19 only 85 to 90 per cent of the process was completed during the time allowed. The length of time required to obtain an accurate value of p_∞ by the above procedure will be considered further in the Discussion section.

The slope, S_∞, of the straight line portion of the $\ln(p - p_\infty)$ versus time plot is

$$S_\infty = \frac{d}{d\theta}\left[\ln(p - p_\infty)\right]_{\theta \to \infty}$$

For desorption it is necessary to exchange p and p_∞ in the definition of S_∞. Values of S_∞ were measured for all of the pressure-time data and tabulated in Table 10 of Appendix II for future reference.

Catalyst Pellet Description

To obtain the catalyst pore volume it is necessary to know both the helium free space and the total volume of the catalyst pellets including pores. The latter is determined by adding mercury under vacuum to a pycnometer filled with catalyst. Since the catalyst is extruded to give cylindrical pellets, it is also possible to measure the average pellet diameter. Table 1 presents the results of these measurements for future reference.

TABLE 1

DESCRIPTION OF AN AVERAGE CYLINDRICAL CATALYST PELLET

Diameter	2.887	mm.
Length	3.014	mm.
Surface Area*	40.78	$mm.^2$
Volume	19.733	$mm.^3$
Weight	0.04882	gm.
Porosity	51.03%	
Pore Length	0.685	mm.
Pore Volume	0.2063	cc./gm.

*External geometrical surface of a pellet

The average pore length listed in Table 1 was calculated from the equation

$$\text{Pore Length} = \frac{\text{Pellet Volume}}{\text{Pellet Surface Area}} \sqrt{2} \ ,$$

which was derived by Wheeler (1C).

EXPERIMENTAL AND THEORETICAL RESULTS

The topics to be considered in this section are the Langmuir isotherm, the short-time data, and diffusion in the catalyst pores. From the Langmuir isotherm the catalyst area, the equilibrium adsorption constant, and the adsorption rate will be found. A consideration of the short-time data will introduce ideas which are important in the discussion of diffusion in the catalyst pores.

Langmuir Isotherm

If n moles of gas are adsorbed per gram of catalyst at pressure p and n_m moles per gram are required to cover the catalyst surface with a complete unimolecular layer, then Langmuir (21 and 22) showed theoretically that

$$\frac{n}{n_m} = \frac{Kp}{1 + Kp} , \qquad (1)$$

where K is the adsorption equilibrium constant. The derivation of Equation (1) based on Langmuir's assumptions is given in Appendix IV. The Langmuir equation may be put in the linear form

$$\frac{p}{n} = \frac{1}{Kn_m} + \frac{1}{n_m} p . \qquad (2)$$

Values of p/n versus p are listed in Table 13 of Appendix III and plotted Fig. 8. While straight lines are not obtained over the entire pressure range the data fits the Langmuir equation reasonably well.

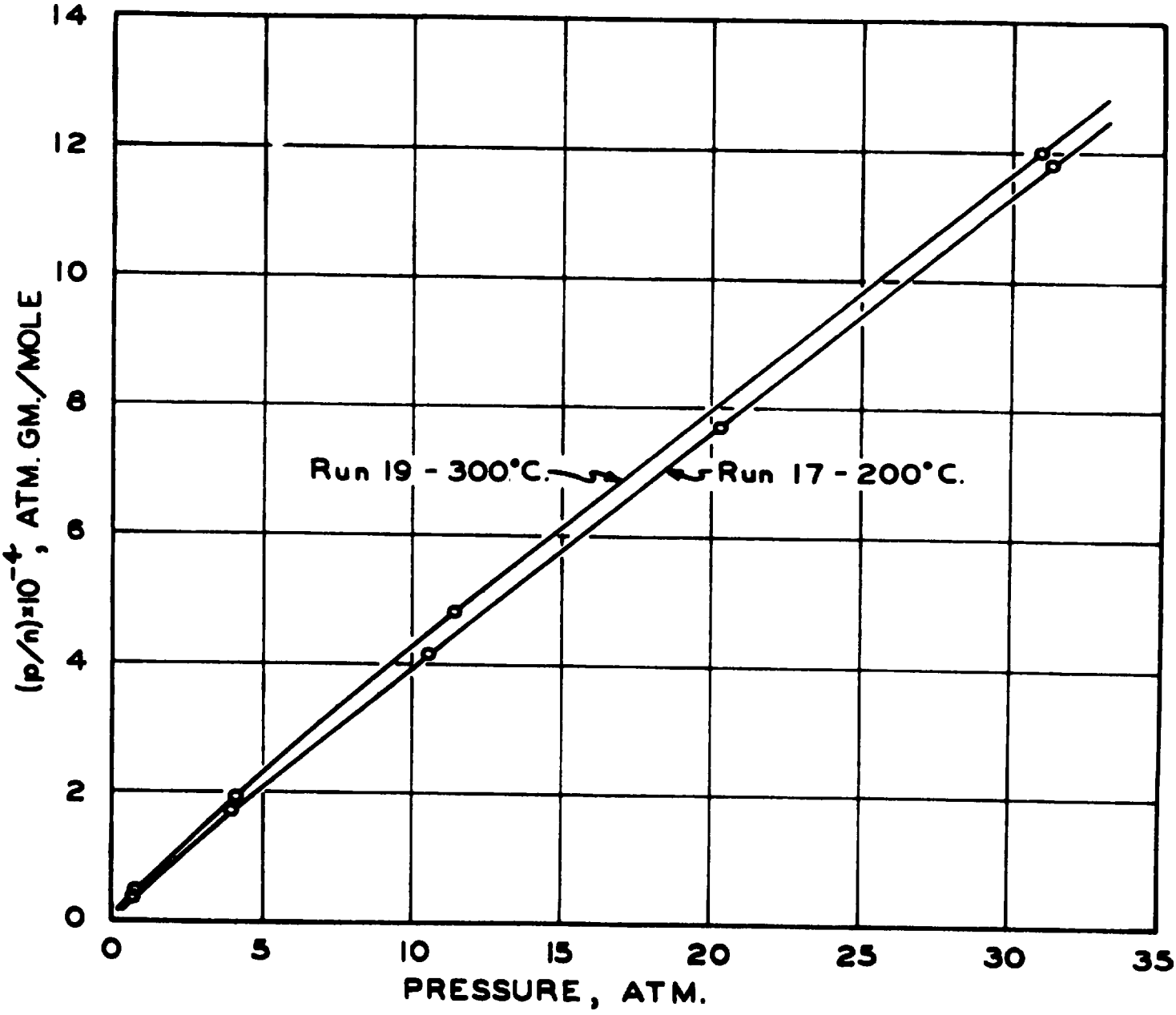

FIG. 8 HYDROGEN ADSORPTION ISOTHERMS PLOTTED ACCORDING TO THE LANGMUIR EQUATION

Catalyst Area: According to Equation (2) the slopes of the isotherms of Fig. 8 are $1/n_m$. By taking the slopes of the 200°C. and 300°C. isotherms at the high-pressure ends it was found that $n_m = 2.70 \times 10^{-4}$ moles/gm. This corresponds to a catalyst surface area of 19.5 $m.^2/gm.$ if the molecular area of hydrogen is taken as 12 $\AA^2$ (1B, p. 161).

Equilibrium Adsorption Constant: The Langmuir equation can be solved for the equilibrium adsorption constant to give

$$K = \frac{n}{p(n_m - n)}$$

Using the value of n_m found above and values of p and n from Table 13, Appendix III, it is possible to calculate K. Reasonably constant values for K of 1.5 $atm.^{-1}$ at 200°C. and 0.75 $atm.^{-1}$ at 300°C. were obtained in the high-pressure region where the Langmuir isotherms are straight lines.

Pursley (28) synthesized methane from carbon monoxide and hydrogen using the same catalyst that was used in this adsorption study. He obtained a value for the hydrogen equilibrium adsorption constant of 1.5 $atm.^{-1}$ between 500°F. (260°C.) and 600°F. (316°C.) and 2 to 27 atm. For the reaction of carbon dioxide and hydrogen on the same catalyst Binder (9) proposed two possible reaction mechanisms and obtained values of 9 and 120 $atm.^{-1}$ for K at 300°C. and one atmosphere and much higher values at lower temperatures. Judging only from the magnitude of the equilibrium adsorption constant, Binder's first mechanism appears to be the more likely one but his high temperature coefficients are not compatible with adsorption data.

Rate of Adsorption: The equilibrium adsorption constant, which was defined as the ratio of the concentration of an adsorbed component to the product of the concentration of the vacant active centers and the equilibrium

pressure of that component, is equal to k/k' where k is the adsorption rate constant and k' is the desorption rate constant. In the derivation of the Langmuir isotherm in Appendix IV it was shown that k can be calculated from experimental data and the kinetic theory of gases. Since K = k/k' and K is known it is also possible to evaluate k' which is more convenient to use in the following discussion. From Appendix IV the desorption rate constant, k', is 6.9×10^{6} sec.$^{-1}$ at 200°C. The next step is to calculate k' from the pressure-time data and compare it with the value obtained from the Langmuir isotherm to see if the observed transient phenomena can be accounted for by the rate of adsorption.

Assume that the net rate of adsorption is the controlling factor at long times and that diffusional gradients are zero in the catalyst pores. The gas occupies a fixed volume $(V_p + \bar{V})$ where V_p is the total pore volume of W grams of catalyst and $\bar{V}$ is the space around the catalyst pellets plus any other volume that may be connected to the catalyst chamber (e.g., the manifold or manifold and burette). The pressure of the gas is p_0' initially, p_∞ at equilibrium, and p at time θ. In Appendix IV the following equation is derived for the net rate of adsorption at constant volume

$$\ln \left[\frac{p - p_\infty}{p_0' - p_\infty} \right] = - k' (1 + F) \theta \quad , \qquad (3)$$

where F is given by the formula

$$F = WnRT/p_\infty (V_p + \bar{V}) \quad .$$

The values of W, T, p_∞, V_p, and $\bar{V}$ are obtained from the experimental data for the adsorption step under consideration and n is found from the adsorption isotherm at p_∞ and T.

The derivative of Equation (3) is

$$\frac{d}{d\theta} \ln (p - p_\infty) = - k' (1 + F) \quad . \tag{4}$$

The term $d \ln(p - p_\infty)/d\theta$ is the slope, S_∞, of the straight line portion of the $\ln(p - p_\infty)$ versus time plot and is tabulated in Appendix II. Using this definition of S_∞ Equation (4) can be put in the form

$$k' = \frac{S_\infty}{1 + F} \quad , \tag{5}$$

which is convenient for evaluating the desorption rate constant.

Values of k' calculated from the experimental data by means of Equation (5) ranged from 1×10^{-6} to 3×10^{-4} per second. The value of k' calculated from the Langmuir isotherm (Appendix IV) was 6.9×10^{-8} per second at 200°C. One must conclude that for the experimental data under consideration adsorption is instantaneous in comparison with the transient phenomena observed.

In order to solve the differential equation leading to Equation (3) it was necessary to make a linearizing approximation. Therefore it is encouraging to note that the solution to the problem at constant pressure (in which no such approximation is required) takes the form

$$\ln \left[\frac{n_\infty - n}{n_\infty - n_0} \right] = - k' \left[1 + \frac{n_\infty}{n_m - n_\infty} \right] \theta \quad ,$$

which is analogous to Equation (3). This equation is easily obtained by integrating Equation (34) of Appendix IV. It was first derived by Langmuir (21) in a slightly different form.

Short-Time Data

It will be recalled that in the $\ln(p - p_\infty)$ versus time plot of Fig. 7 the data described a curve which became a straight line at long times but deviated sharply from this straight line at short times. Further consideration of this short-time data leads to some interesting results.

A method of representing the short-time data, which proved to be unsuccessful, was based on an empirical approach to the problem. A curve with a shape similar to that of Fig. 7 can often be represented by the sum of two exponential terms with widely different half-lives. At long times one exponential term should vanish leaving the exponential which gives the straight line in Fig. 7. If one of the exponentials is known then the other can be found from their sum at short times. Although Forster (8) expressed some of the results of his adsorption rate studies by this means it was of little use in the present investigation. When the long-time exponential was subtracted from the pressure-time data is was found that the result was not a straight line but another curve similar to Fig. 7.

Diffusion of gas in the catalyst pores was considered a possible explanation for the variation of pressure with time. Liebhafsky (24) showed that at short times a diffusional process depends upon the square-root of time. Plots of pressure versus the square-root of time were tried and found to give a straight line through the first few points. Fig. 9 is an example of such a plot. Values of the initial pressure, p_i, obtained by extrapolating to zero time were recorded in Table 10 of Appendix II.

It is convenient to define a function S_1 by the equation

$$S_1 = \left[\frac{-1}{p_1 - p_0}\right]\left[\frac{dp}{d\sqrt{\theta}}\right]_{\theta \to 0}$$

where $(dp/d\sqrt{\theta})_0$ is the slope of the straight line portion of the pressure versus square-root of time plot. Although S_1 differs by the factor $(p_0 - p_1)$ from the true initial slope of this plot it will be referred to as the "initial slope". Values of S_1 are listed in Table 10 of Appendix II.

The pressures p_0 , p_0' , p_1 and p_2 will be defined in this paragraph and henceforth referred to only by symbol. These pressures are displayed graphically in Figs. 7 and 9. The initial pressure in the adsorbent chamber before any gas is added (or withdrawn) is p_0. This is the equilibrium pressure of the previous point. If a quantity of gas were admitted to the catalyst and it occupied the volume of the system, $(\overline{V} + V_p)$, without adsorbing, the pressure would be p_0'. This pressure can be calculated from the experimental data. Apparently, however, there is a certain amount of instantaneous adsorption since the extrapolation of the pressure versus square-root of time data to zero time does not give p_0' but a pressure, p_1, which is much less than p_0'. If the straight line through the long-time data of a $\ln(p - p_\infty)$ versus time plot is extrapolated to zero time a pressure p_2 is defined. This pressure lies somewhere between p_1 and p_∞ but has no physical significance. The record of a pressure recorder connected to the adsorbent chamber would jump from p_0 to p_1 when a quantity of gas was admitted to the adsorbent chamber and then drop off with time, approaching p_∞ asymptotically.

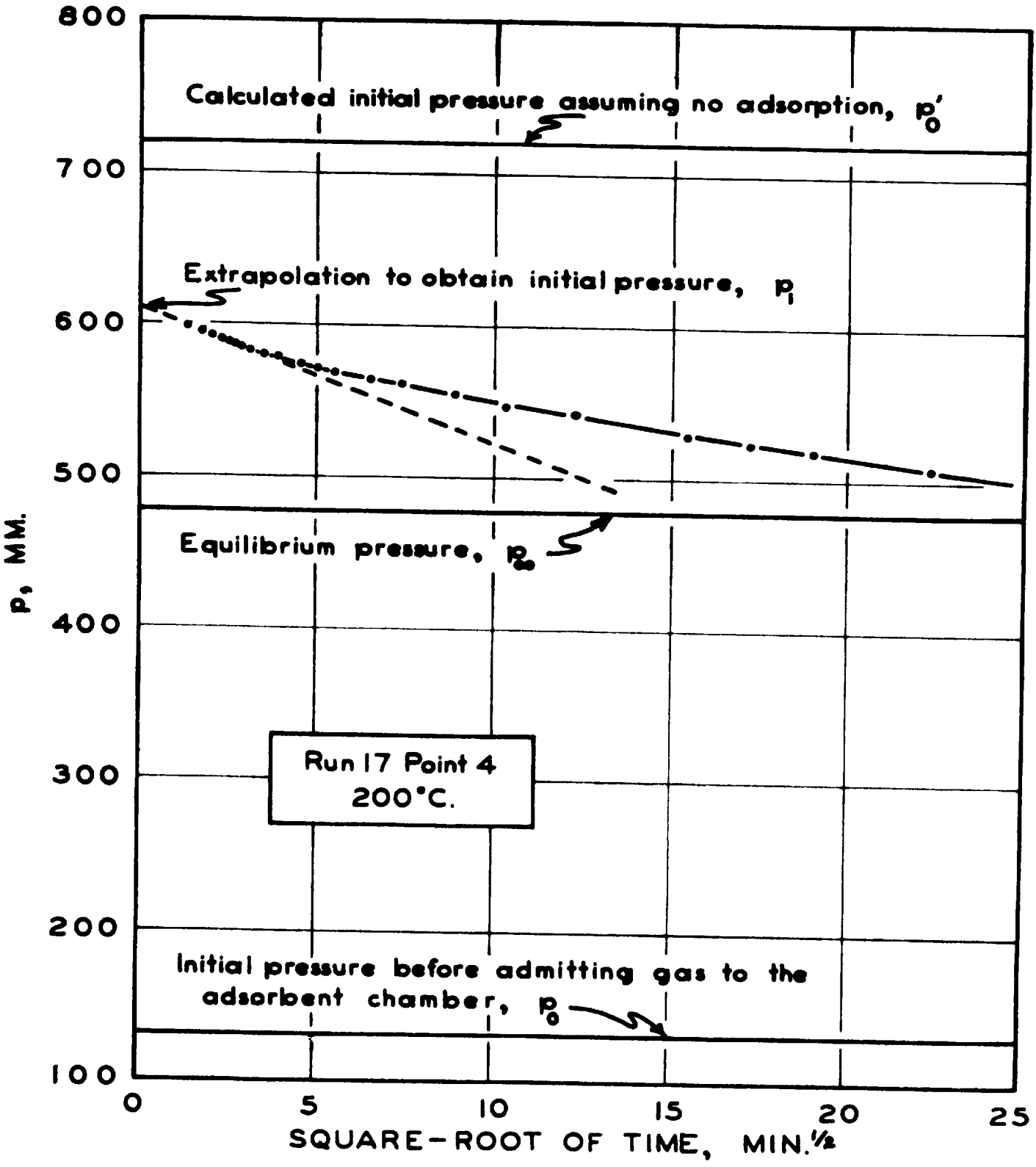

FIG. 9 DETERMINATION OF THE INITIAL PRESSURE

Readily Accessible Surface: The fact that p_1 does not coincide with p_0' but lies between p_0' and p_∞ indicates that a certain fraction, f, of the catalyst surface is readily accessible. If n_0 moles of gas per gram of catalyst are adsorbed on W grams of catalyst at p_0 then fWn_0 is the moles of gas adsorbed on the readily accessible portion of the surface before gas is admitted to the adsorbent chamber. Likewise fWn_1 moles of gas are adsorbed on the same fraction of the surface just after gas is admitted to the adsorbent chamber. Therefore

$$fW(n_1 - n_0) = \text{(The moles of gas initially adsorbed)} \quad . \qquad (6)$$

By calculating the moles of gas initially adsorbed from the experimental data and taking values of n_0 and n_1 from the adsorption isotherms plotted in Fig. 6 it is possible to compute f from Equation (6). The results of such computations are summarized in Table 14 of Appendix III and shown in Fig. 10. Although f seems to show some trend with pressure it will be sufficient for the purposes of this study to take an average value of f equal to 0.5.

High-Pressure Catalyst Reduction: A glance at Runs 15, 18, and 20 on Fig. 6 shows that the high-pressure reduction which took place after Run 15 increased the adsorption by about 25 per cent. An increase in the catalyst free space was also observed after the high-pressure reduction. If these increases in catalyst area and pore volume are assumed to be due to the opening of small pores, then it is possible to estimate the size of these pores. For cylindrical catalyst pores the average hydraulic radius, r, of the pores is related to the pore volume, V_p, and surface area, A, by the equation

$$r = V_p/A \quad . \qquad (7)$$

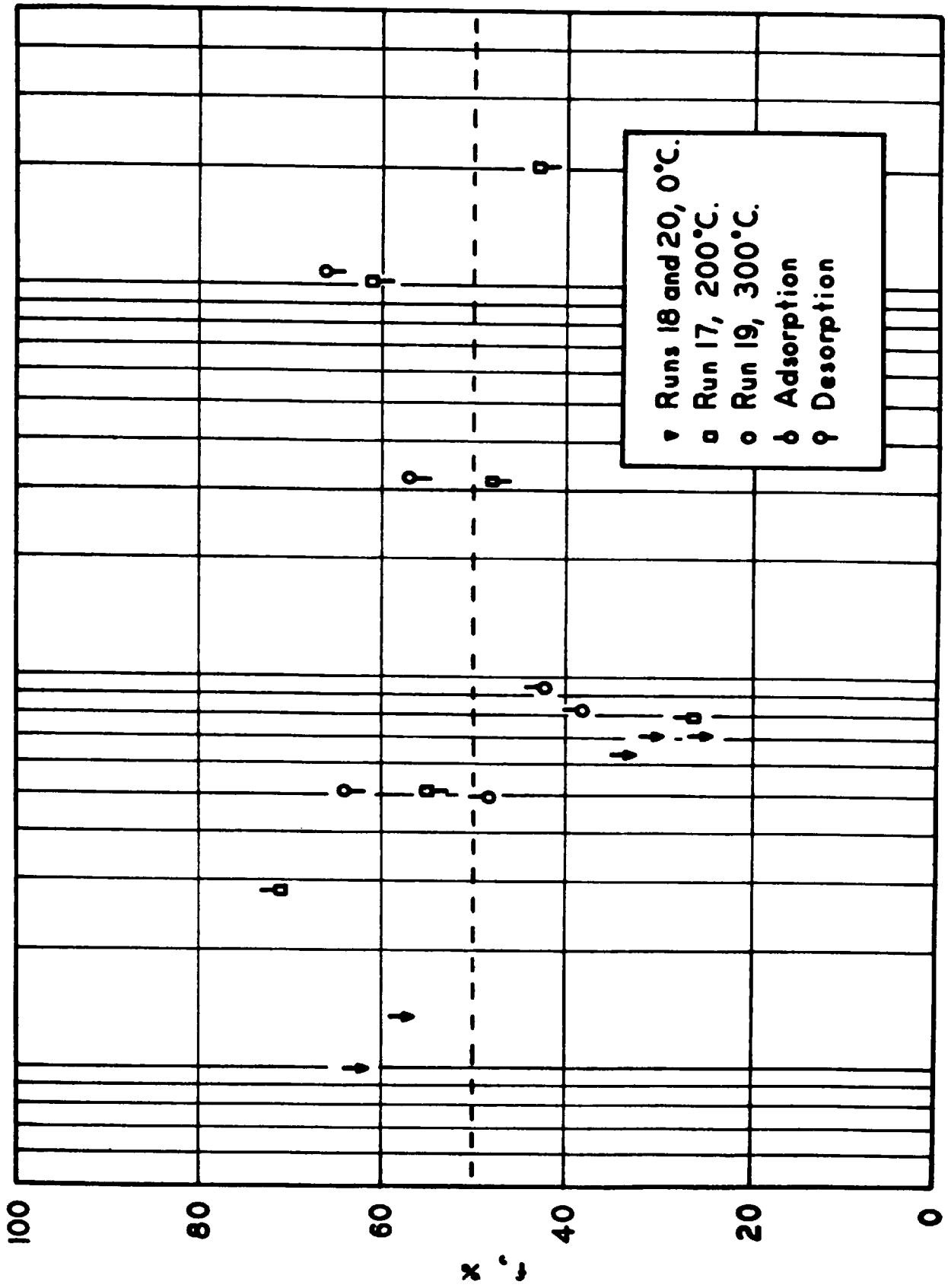

FIG. 10 FRACTION OF CATALYST SURFACE READILY ACCESSIBLE

Wheeler (1C) gives a more accurate form of Equation (7) which includes factors correcting for porosity and surface roughness but he points out these factors tend to cancel one another. The 25 per cent increase in surface area due to high-pressure reduction is equivalent to 20 per cent of the resulting area. Since the catalyst area is 19.5 $m.^2/gm.$ the increase in area is 3.90 $m.^2/gm.$ The pore volume was 0.2032 cc./gm. before high-pressure reduction and 0.2063 cc./gm. afterwards so that the volume increase is 0.0031 cc./gm. Thus the average hydraulic radius of the fine pores which were opened up is

$$r = 0.0031/3.90x10^4 = 8x10^{-8} \text{ cm. or } 8 \text{ Å} .$$

For comparison it should be noted that the diameter of a hydrogen molecule is 3.8 Å (10, p. 367) and the average hydraulic radius of the entire catalyst pore structure is

$$r = 0.2063/19.5x10^4 = 106 \text{ Å} ,$$

or 424 Å diameter.

Diffusion in Catalyst Pores

It is known that diffusional effects depend upon the square-root of time at short times and are exponential in time at long times. Piret et al. (26) used both types of time plots in their study of liquid diffusion rates in porous solids. The data of this investigation show a similar behavior. Possible diffusional mechanisms in the present case include diffusion of hydrogen into pores or into the solid material itself and the dissipation of heat generated by the adsorption of hydrogen. In the example chosen for Figs. 7 and 9 the heat of adsorption is sufficient to raise the temperature of the catalyst and the gas surrounding it

°C. This would raise the pressure in the burette by about one millimeter which is negligible compared to the observed variation. In the same example the solution of hydrogen by the nickel in the catalyst (15) would likewise change the pressure only one millimeter. Thus the diffusion of hydrogen into the catalyst pores appears to be the most likely mechanism. The following paragraphs will be devoted to developing the picture of diffusion and adsorption in the catalyst pores, describing the process with a differential equation and boundary conditions, solving this boundary value problem, and investigating the solution.

It is customary to divide the pore space of a porous catalyst into macropores and micropores. According to Brunauer (10, p. 376) "the present usage is to call micropores those that have radii smaller than 100 Å" ($r < 50$ Å). Wicke (34) proposed that short micropores surround the macropores like fjords and that their surface area was 1000 times that of the macropores. When gas is admitted to the catalyst the short micropores fill rapidly and the slow process is the diffusion in the macropores which must transport all the gas that is adsorbing on the micropore walls. However, Wicke's picture is not in accordance with the phenomenon of the readily accessible surface, Fig. 10, wherein one-half of the surface was reached immediately.

If half of the catalyst surface is readily accessible then the macropores must contain this surface area and the slow process is diffusion in the micropores. Therefore, the process that takes place when a quantity of gas is admitted to the catalyst chamber may be described in the following manner. The gas admitted increases the pressure, p_0 of the system which includes the macropores to p_1 and adsorbs immediately on macropore walls. Then the gas slowly diffuses into the micropores

and adsorbs on the micropore walls. This causes the pressure in the micropores and surrounding system to drop from p_1 to p_∞ while the average micropore pressure increases from p_0 to p_∞.

It is convenient to use concentrations instead of pressures to describe the diffusional process. Let $y(x,\theta)$ moles per unit volume be the concentration in a micropore at a distance x from the micropore mouth at time θ. Then the average concentration in a micropore is

$$y(\theta) = \frac{\int_0^L y(x,\theta)\, dx}{\int_0^L dx}$$

where L is the average length of the micropores. The concentration in the volume, $\bar{V}$, external to the micropores is $\bar{y}(\theta)$. The concentrations $\bar{y}(\theta)$, $\bar{y}_0$, $\bar{y}_1$, and $\bar{y}_\infty$ correspond to the pressures p, p_0, p_1, and p_∞. Since $\bar{y} = y$ at equilibrium, $\bar{y}_\infty = y_\infty$ and $\bar{y}_0 = y_0$.

In preparing a mathematical statement of the diffusional process the catalyst pore structure will be described with the aid of the following symbols. The symbol V_p, which was previously used for the entire pore volume, will henceforth refer only to the micropore volume. The volume $\bar{V}$ refers to the sum of the macropore volume, the space surrounding the catalyst, and any other volumes connected to the adsorbent chamber. If the total surface area of W grams of catalyst is A, then the surface area of the macropores is fA and the micropores (1-f)A. The micropore surface area may also be written V_p/r where r is the average hydraulic radius of the micropores.

To facilitate the mathematical description of adsorption on the catalyst the adsorption isotherm will be approximated by a straight line

between the pressures p_0 and p_1. If n' moles of adsorbate per unit area of catalyst are in equilibrium with the gas concentration y, then the approximate isotherm is

$$n' = b + cy \quad ,$$

and

$$\Delta n' = c \Delta y \quad . \tag{8}$$

Substituting $p = RTy$ and $\Delta n' = Wn$ in Equation (8) gives

$$c = (WRT/A)(dn/dp) \quad , \tag{9}$$

where (dn/dp) is the average slope of the adsorption isotherm between p_0 and p_1.

In order to follow the diffusion of gas in the micropores experimentally, the average micropore pressure must be related to the observed pressure change between p_1 and p_∞. This relationship is provided by a material balance. Initially, $\overline{Vy}_1$ moles of gas occupy the volume $\overline{V}$ and at time θ there are $\overline{Vy}(\theta)$ moles of gas in $\overline{V}$. Thus

$$\overline{V}\left[\overline{y}_1 - \overline{y}(\theta)\right] = \text{decrease in moles of gas occupying } \overline{V} \quad .$$

Likewise, $V_p\, y_0$ moles of gas occupy the micropore volume V_p initially and at time θ there are $V_p y(\theta)$ moles of gas in V_p so that

$$V_p\left[y(\theta) - y_0\right] = \text{increase in moles of gas occupying } V_p \quad .$$

Substituting Equation (8) in the expression $(fA)\Delta n'$, which is the increase in moles adsorbed on the macropore walls, and in $(V_p/r)\Delta n'$, which is the increase in moles adsorbed on the micropore walls, gives

$$cfA\left[\overline{y}_1 - \overline{y}(\theta)\right] = \text{decrease in moles of gas adsorbed on the macropore walls} \quad ,$$

and

$$(cV_p/r)\left[y(\theta) - y_0\right] = \text{increase in moles of gas adsorbed on micropore walls} .$$

Summing up terms

$$\left[\bar{y}_1 - \bar{y}(\theta)\right] = B\left[y(\theta) - y_0\right] . \tag{10}$$

Where

$$B = V_p\,(1 + c/r)/\bar{V}(1 + cfA/\bar{V}) . \tag{11}$$

Substituting $r = V_p/(1 - f)A$ and Equation (9) into Equation (11) gives

$$B = \frac{V_p/\bar{V} + (1 - f)\,E}{1 + f\,E} , \tag{12}$$

where

$$E = (WRT/\bar{V})(dn/dp) . \tag{13}$$

The dimensionless constant, E, can be calculated from the experimental data and the average slope of the adsorption isotherm (dn/dp) between p_0 and p_1. Since the term $V_p/\bar{V}$ is small compared to (1 - f)E it can be neglected and material balance constant, B, can be evaluated using Equation (12). At equilibrium Equation (10) becomes

$$(\bar{y}_1 - \bar{y}_\infty) = B(y_\infty - y_0) ,$$

or

$$B = (p_1 - p_\infty)/(p_\infty - p_0) , \tag{14}$$

which provides an alternate method for calculating B.

The foregoing paragraphs have been devoted to developing the picture of diffusion and adsorption in the catalyst pores and it is now possible to proceed with a mathematical description of the process. It will be assumed that diffusion is one dimensional and that the diffusivity,

P_0 is constant. The partial differential equation for the diffusion of gas in a micropore accompanied by adsorption on the micropore walls is

$$D \frac{\partial^2}{\partial x^2} y(x,\theta) = (1 + c/r) \frac{\partial}{\partial \theta} y(x,\theta) \quad .$$

For dead end pores of length L or open ended pores of length 2L

$$D \frac{\partial}{\partial x} y(L,\theta) = 0 \quad ,$$

and at the mouth of the micropores the gas concentration is in equilibrium with the macropore and surrounding gas concentration so that

$$y(0,\theta) = \bar{y}(\theta) \quad .$$

The initial concentration in the catalyst pores is

$$y(x,\theta) = y_0 \quad .$$

These boundary conditions together with the differential equation constitute the following boundary value problem:

$$\left.\begin{aligned} D \frac{\partial^2}{\partial x^2} y(x,\theta) &= (1 + c/r) \frac{\partial}{\partial \theta} y(x,\theta) \\ y(x,0) &= y_0 \\ \frac{\partial}{\partial x} y(L,\theta) &= 0 \\ y(0,\theta) &= \bar{y}(\theta) \end{aligned}\right\} \qquad (15)$$

The solution of Boundary Value Problem 15 is

$$\left[\frac{p - p_\infty}{p_1 - p_0}\right] = \sum_{j=0}^{j=\infty} \left[\frac{2\bar{B}}{\bar{B} + \bar{B}^2 + \bar{\beta}_j^2}\right] e^{-\beta_j^2 t} \quad , \qquad (16)$$

where

$$t = D\theta/L^2(1 + c/r) \quad , \qquad (17)$$

and $\beta_1, \beta_2, \beta_3, \ldots$ are the positive roots of

$$\beta_j \cot \beta_j + B = 0 \quad . \tag{18}$$

The details of the solution are given in Appendix IV. In the dimensionless form Hatta's (16) solution for the extraction of a liquid from a solid by a finite volume of solvent may be integrated and rearranged to give Equation (16). The first six roots of Equation (18) are tabulated in Appendix IV of Carslaw and Jaeger (12).

When the exponent $\beta_j^2 t$ becomes large only the first term of the infinite series in Equation (16) is significant and the equation reduces to

$$\ln \left[\frac{p - p_\infty}{p_1 - p_0} \right] = \ln \left[\frac{2B}{B + B^2 + \beta_1^2} \right] - \beta_1^2 t \quad . \tag{19}$$

Substituting Equation (17) in Equation (19) and taking the derivative with respect to time yields

$$\frac{d}{d\theta} \ln (p - p_\infty) = - \beta_1^2 D/L^2 (1 + c/r) \quad . \tag{19}$$

The term $d \ln(p - p_\infty)/d\theta$ is the slope S_∞ of the pressure-time plots at long times. Substituting the equation for S_∞ and Equations (9) and (15) in Equation (19) gives after rearranging

$$(V_p D/L^2) = - (\bar{V} S_\infty/\beta_1^2) \left[V_p/\bar{V} + (1 - f)E \right] \quad . \tag{20}$$

In Equation (20) all the unknown terms (i.e., $V_p D/L^2$) are grouped together on one side of the equation with the exception of the term $V_p/\bar{V}$. Subsequent information shows that $V_p/\bar{V}$ may be neglected without introducing more than 20 per cent error. The term β_1 is the first root of the equation

$$\beta_j \cot \beta_j + B = 0 \quad . \tag{18}$$

Recalling that

$$B = \frac{V_p/\bar{V} + (1 - f)\,E}{1 + f\,E} \quad , \tag{12}$$

and

$$E = (WRT/\bar{V})(dn/dp) \quad , \tag{13}$$

it is possible to calculate the term $(V_p D/L^2)$ from experimental data using Equation (20). Although Equation (20) was derived assuming that the slope of the adsorption isotherm, (dn/dp), used to calculate E had a constant value between p_0 and p_1, in most cases this slope varies considerably. Therefore it seemed preferable to evaluate E at p_∞ in Equation (20). Tables 16 and 17 of Appendix III show the calculations based on Equation (20). The results are divided by W to put them on a unit weight basis and are plotted in Fig. 11. The unexpected variation of $(V_p D/WL^2)$ with pressure shown in Fig. 11 is probably due to the fact that the dividing line between macropores and micropores is itself a variable.

At small values of t the series solution of Equation (16) converges so slowly that it is difficult to evaluate. The approximate solution

$$(p_1 - p)/(p_1 - p_0) = 2B\,(t/\pi)^{1/2} \quad , \tag{21}$$

valid at small t, is derived in Appendix IV. Substituting Equation (17) in Equation (21) and taking the derivative with respect to the square-root of time yields

$$\left[-1/(p_1 - p_0)\right]\,(dp/d\theta^{1/2}) = 2B\left[D/\pi L^2\,(1 + c/r)\right]^{1/2} \quad . \tag{22}$$

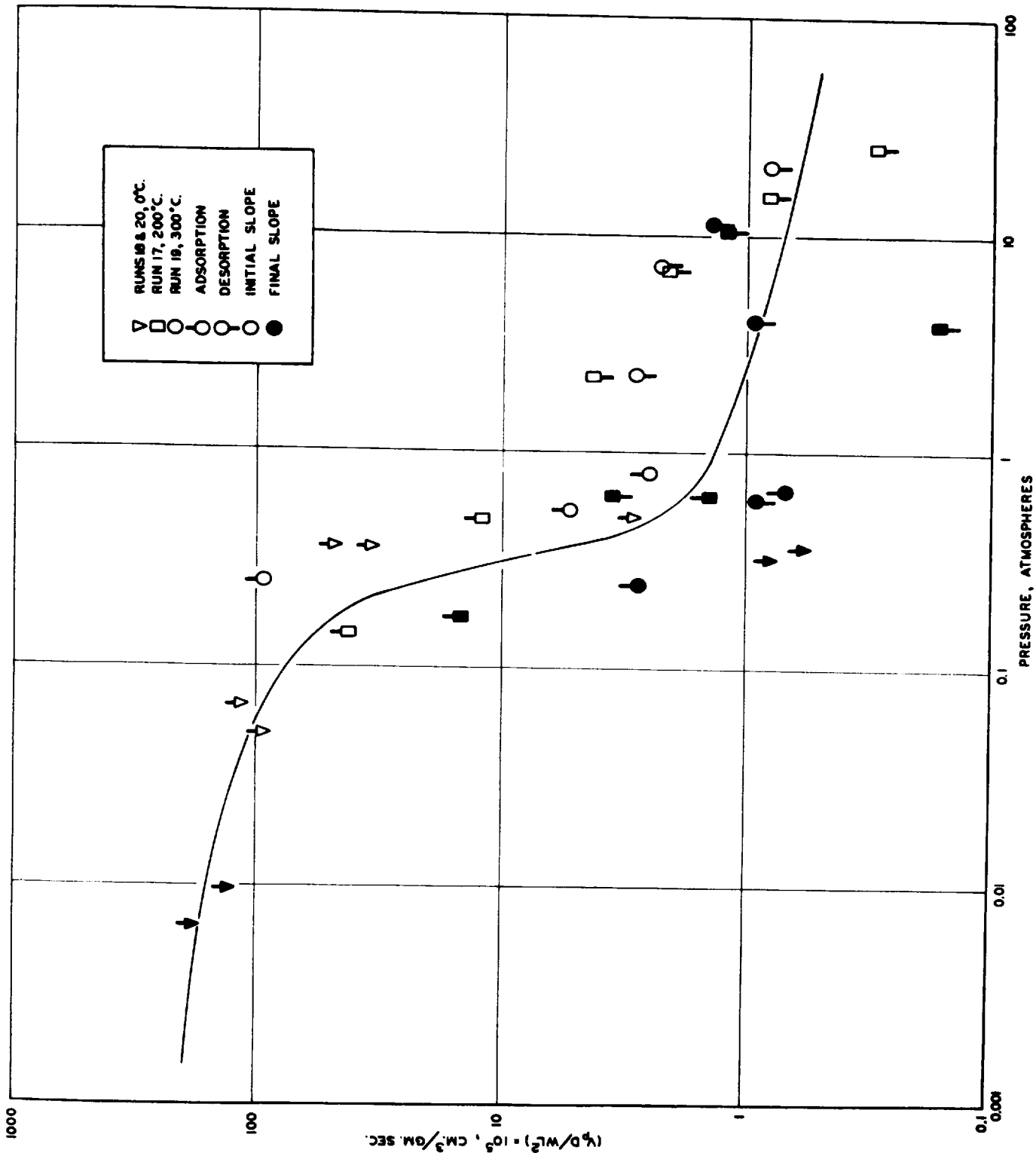

FIG. 11 VARIATION OF (V_pD/WL^2) WITH PRESSURE

The term $-dp/(p_1 - p_0)d\theta^{1/2}$ is the slope S_1 of pressure-time plot at short times. Substituting the equation for S_1 and Equations (9) and (13) in Equation (22) gives after rearranging

$$(V_p D/L^2) = (\pi \bar{V} S_1^2/4) \left[- \frac{(1 + f E)^2}{V_p/\bar{V} + (1 - f) E} \right] . \qquad (23)$$

Equation (23) is the short-time analogue of Equation (20) and the term $(V_p D/L^2)$ may be calculated as before. However, in these calculations there is again the question as to the pressure at which the slope of the adsorption isotherm, (dn/dp), used to calculate E should be evaluated. Since initially the pressure in the micropores is somewhere between p_0 and p_1, the term (1 - f)E in Equation (23) which represents adsorption on the micropore walls was evaluated at $(p_0 + p_1)/2$. Likewise, since the initial pressure in the macropores is p_1, the term fE in Equation (23) which represents adsorption on the macropore walls was evaluated at p_1. Tables 15 and 17 of Appendix III show the calculations based on Equation (23) and the results are plotted in Fig. 11. The superposition of the term $(V_p D/WL^2)$ calculated from the initial slope data upon the same term calculated from the long-time slope data shown in Fig. 11, tend to indicate that the concept of the catalyst pore structure developed here may be valid. However, other evidence can be brought to bear. A comparison of the constant B evaluated by different methods can be made and the term $(V_p D/WL^2)$ can be checked by an order-of-magnitude calculation.

Comparison of B Values: The constant B defined by Equations (12) and (14) originated when a material balance was made between gas in the micropores and gas in the remaining space. Values of B computed according to Equation (14)

$$B = (p_1 - p_\infty)/(p_\infty - p_0) , \qquad (14)$$

represent an average value between p_0 and p_1 and are tabulated in column of Table 2.

The constant B can also be calculated in a manner that is independent of Equations (12) and (14). Equation (19),

$$\ln\left[\frac{p - p_\infty}{p_1 - p_0}\right] = \ln\left[\frac{2B}{B + B^2 + \beta_1^2}\right] - \beta_1^2 t \quad , \tag{19}$$

is the equation of the straight line portion of the $\ln(p - p_\infty)$ versus time plot previously described (Fig. 7). If this straight line is extrapolated to zero time the intercept is

$$(p_2 - p_\infty)/(p_1 - p_0) = (2B)/(B + B^2 + \beta_1^2) \quad . \tag{24}$$

Values of p_2 were determined along with p_∞ and S_∞ from the semi-logarithmic plots of the pressure-time data and recorded in Table 10 of Appendix II. Solving Equation (24) simultaneously with the equation

$$\beta_1 \cot \beta_1 + B = 0 \quad ,$$

yields two values of B which are listed in columns 6 and 7 of Table 2. The values of B presented in column 5 should agree with the values in either column 6 or 7 if (1) the slope of the adsorption isotherm were constant between p_0 and p_1, (2) Equation (16) and the assumptions leading to it were correct, and (3) the pressures p_0, p_1, p_2, and p_∞ were accurately determined. The fact that reasonable agreement was obtained in Table 2 even though the slope of the adsorption isotherm is not at all constant tends to substantiate the procedures and assumptions used here.

For comparison values of B calculated by Equation (12) are shown in columns 4 and 8 of Table 2. Column 8 is based on the calculations of used in evaluating $(V_p D/L^2)$ from S_∞ and therefore represents the value

TABLE 2

COMPARISON OF VALUES OF B CALCULATED BY DIFFERENT METHODS

			Method of Calculating B				
p_0 atm.	p_∞ atm.	p_1 atm.	S_1	$\left[\frac{p_1-p_\infty}{p_\infty-p_0}\right]$	$\left[\frac{p_2-p_\infty}{p_1-p_0}\right]$ First Solution	$\left[\frac{p_2-p_\infty}{p_1-p_0}\right]$ Second Solution	S_∞
(1)	(2)	(3)	(4)	(5)	(6)	(7)	(8)
Run 17 - 200°C.							
0	0.1714	0.2863	1.035	0.670	0.280	(10.5)	0.440
0.1714	0.626c	0.7988	0.259	0.380	0.301	(9.6)	0.147
3.932	0.6259	0.5141	0.041	0.034	0.018	...	0.147
10.49	3.932	3.211	0.115	0.110	0.063	...	0.178
0.23	10.49	10.21	0.038	0.029	0.021	...	0.062
Run 18 - 0°C.							
0	0.0066	0.0996	3.79	14.1	(0.230)	14.6	0.917
0.0066	0.3658	0.7126	0.380	0.966	0.326	8.95	0.122
Run 19 - 300°C.							
0	0.2448	0.4980	0.684	1.04	0.315	(9.2)	0.367
0.2448	0.6694	0.8345	0.236	0.389	0.388	(7.6)	0.152
4.082	0.6104	0.5163	0.042	0.027	0.013	...	0.165
11.40	4.082	3.251	0.143	0.114	0.050	...	0.216
30.99	11.40	10.87	0.043	0.027	0.013	...	0.081
Run 20 - 0°C.							
0	0.0097	0.1350	3.16	12.9	(0.197)	14.1	0.902
0.0097	0.3263	0.7093	0.414	1.21	0.388	7.6	0.155

of B at p_∞. Column 4 is similarly related to S_1 and therefore represents the value of B somewhere between p_0 and p_1.

Diffusivity: In the following paragraphs the order of magnitude of the term $(V_p D/WL^2)$ will be estimated for comparison with the results shown in Fig. 11. It should be borne in mind that the diffusional process being examined pertains to the transport of a single component in fine pores.

The rate of diffusion per unit cross-sectional area is proportional to the concentration gradient and the proportionality constant is called the diffusivity. In Poiseuille (stream-lined) flow through a tube with a hydraulic radius r, the diffusivity is

$$D = (r^2 p/2\mu) + (4rv/3) \quad ,$$

for a gas with viscosity μ and mean molecular velocity v. The term (4rv/3) corrects for slip at the walls and is usually neglected but at small r or p it becomes important. In fine capillaries when only the term 4rv/3 is significant the method of transport is termed Knudsen or molecular flow. For hydrogen flowing in a 100-Å diameter (r = 25 Å) pore at 200°C. and 30 atmospheres, the Knudsen term is about ten times the Poiseuille term. Since the Knudsen diffusivity is independent of pressure the original assumption of constant diffusivity is justified.

Since $V_p = (1 - f)\,Ar$ and $D = 4rv/3$ the term $(V_p D/WL^2)$ can be written

$$(V_p D/WL^2) = \left[4(1 - f)Av/3W\right] (r/L)^2 \quad , \qquad (25)$$

or

$$V_p D/WL^2 = \left[(4)(0.5)(19.5\text{x}10^4)(2.23\text{x}10^5)/3\right] (r/L)^2 \quad ,$$

$$V_p D/WL^2 = 2.90\ (r/L)^2 \text{x}10^{10} \text{ cc./gm.-sec.} \quad ,$$

for hydrogen at 200°C. If the average pore length given in Table 1 is used for the micropore length and r is assumed to be $1\text{x}10^{-8}$ cm. which is the minimum sized hole through which a hydrogen molecule can pass then

$$V_p D/WL^2 = 62\text{x}10^{-5} \text{ cc./gm.-sec.} \quad .$$

Although this is a minimum value it is still a hundredfold greater than most of the data in Fig. 11. The discrepancy might be accounted for by

two corrections to Knudsen-type diffusivity which have been proposed. Barrer (4) pointed out that if the lifetime of a molecule in the adsorbed state becomes appreciable compared with the time of transit through a tube, it is necessary to correct D according to the formula

$$D = (4rv/3)(1 + \tau v/12r)^{-1} \quad . \qquad (26)$$

The average life of an adsorbed molecule, τ, can be estimated from the Langmuir isotherm. In Appendix IV a value of 1.4×10^{-9} sec. at 200°C. was found for τ based on the high-pressure portion of the 200°C. isotherm. The correction factor becomes

$$\tau v/12r = 2600 \quad ,$$

which more than compensates for the high value of $V_p D/WL^2$ originally calculated.

The second factor affecting flow in fine pores is surface migration of the adsorbed molecules. This effect tends to increase the diffusivity but it is probably of more importance for multimolecularly adsorbed molecules where the second and higher layers are loosely held. Recent investigators of surface migration are Carman and Malherbe (11) and Jones (18) while summaries of earlier data may be found in Wheeler (1C), Brunauer (10, chapter 13) and Barrer (5, chapter 8).

Micropore Size: It is possible to obtain an idea of the micropore size by inserting the corrected Knudsen diffusivity in the value of $V_p D/WL^2$ taken from Fig. 11. Correcting Equation (25) by the factor $(12r/\tau v)$ from Equation (26) gives

$$V_p D/WL^2 = 16(1 - f)Ar^3/W\tau L^2 \quad ,$$

and

$$1\times10^{-5} = 16(0.5)(19.5\times10^{4})r^{3}/(1.4\times10^{-9})(0.0685)^{2}$$

$$r = 3.5\text{Å} \quad .$$

This value of r is probably a maximum since the length of the micropores alone should be less than the total pore length listed in Table 1. The corresponding micropore volume is 0.0034 cc./gm. which is 1.6 per cent of the total pore volume.

Effusion in Catalyst Pores: It is interesting to speculate upon the assumptions made regarding the geometry of catalyst micropores. During Ritter and Drake's (29) study of macropore-size distributions of various materials using their high-pressure mercury-penetration method they found that 99 per cent of the mercury was retained by their kieselguhr sample after the pressure was released and the sample was shaken. This was attributed to "ink-bottle"-type pores which tended to retain the mercury.

Suppose instead of cylindrical pores the catalyst consisted of rows of chambers, connected by small orifices. Gas flow would then be controlled by the rate of effusion through the small orifices between the chambers. A difference-differential equation representing effusion and adsorption in catalyst micropores is derived in Appendix IV. If differences are approximated by derivatives the problem becomes identical to the diffusional problem already solved providing the definition of t given by Equation (17) is replaced by

$$t = \frac{\pi r_{o}^{2} v\, N\theta}{J\, V_{p}\, (1 + c/r)} \quad , \tag{27}$$

where

v = mean molecular velocity

J = average number of connecting microchambers in a row

N = number of rows of connecting microchambers

r = average hydraulic radius of the orifices between microchambers.

Thus $(V_p D/L^2)$ must be replaced by $(\pi r_0^2 vN/J)$ in Equations (20) and (23) for pore geometry in which there is effusion.

Diffusion and effusion may be compared with the help of the following considerations. If the connecting chambers comprising the micropore structure are assumed to be spherical then the chamber length is 6r and the length of a row of chambers is

$$L = 6rJ \quad . \tag{28}$$

In Equation (28) it is tacitly assumed that the loss in chamber wall area due to orifices connecting with lateral chambers is compensated by the increase due to surface roughness. The volume of N cylindrical micropores is

$$V_p = 4\pi r^2 LN \quad , \tag{29}$$

and the diffusivity in a long tube is

$$D = 4rv/3 \quad , \tag{30}$$

for Knudsen-type flow (molecular streaming). Substituting Equations (28, 29, and 30) into Equation (27) gives

$$tL^2 (1 + c/r)/\theta = (9/8)(r_0/r)^2 D \quad . \tag{31}$$

Rearranging Equation (17) gives

$$tL^2 (1 + c/r)/\theta = D \quad . \tag{32}$$

A comparison of Equation (31) from the effusion study and Equation (32) from the diffusion study shows the diffusivities differ by a factor of about $(r_o/r)^2$. Thus if the flow mechanism in small pores is effusion between microchambers instead of Knudsen-type diffusion in cylindrical pores, the problem can still be analyzed assuming equivalent cylindrical pores but the Knudsen diffusivity should be reduced by the factor $(r_o/r)^2$. In the present case the average hydraulic radius of the micropores, r, approaches molecular dimensions as a minimum value so that even if the correction $(r_o/r)^2$ were necessary it would be nearly unity.

Diffusion of Helium: A very interesting run was made in which helium at 500 psig. was suddenly vented from the catalyst, the system sealed, and the pressure rise followed on the manometer. The data were similar to those obtained whenever hydrogen was desorbed but the magnitude of the pressure changes were greatly reduced. Equations (20) and (23) still apply, of course, but now E is zero. By eliminating the (V_pD/L^2) term between the two equations it is possible to solve for V_p. The result is 0.0013 cc./gm. which corresponds to a pore diameter of 6 Å. By using this value of V_p in either Equation (20) or (23) it is found that $V_pD/WL^2 = 0.0053 \times 10^{-5}$ cc./gm.-sec. This is a surprising result. Since helium has negligible adsorption the corrections to the Knudsen diffusivity are both zero and helium should give a value of $V_pD/WL^2 = 30 \times 10^{-5}$ cc./gm.-sec. at 0°C.

Prior to the helium run the catalyst was accidentally contaminated with some mercury from the dead weight tester mercury leg. This was removed by high-temperature evacuation before the helium run but it does place the data under suspicion.

DISCUSSION

It was convenient to include much of the discussion of the results in the section on the experimental and theoretical results. However, it is easier to discuss some points using the background of the entire theoretical section. Those points will be considered here following a discussion of the apparatus.

Apparatus

Both volumetric and gravimetric methods were considered for measuring the required gas adsorption isotherms. Although the gravimetric method is frequently used for measuring high-pressure adsorption it was rejected in this case because it was not suited to high-pressure (30 atm.) measurements at high temperature (400°C.). The disadvantage of the volumetric method is that at high pressures the adsorption is small compared to the quantity of gas in the free space of the adsorbent chamber and connecting tubing. As was pointed out in the Apparatus section, this results in the determination of the quantity of gas adsorbed by the difference of two large numbers. To minimize this effect the adsorbent chamber was scaled up by a factor of about one hundred over the conventional size of volumetric adsorption apparatus.

Another interesting feature of the equipment was the use of a dead weight gage tester to measure pressures above one atmosphere. By connecting this tester to the system with a mercury leg and a mercury level indicator (tuning eye contact indicator) it was possible to detect pressure changes of 0.1 psi. at 500 psi. This equipment design facilitated

the measurement not only of adsorption isotherms but also adsorption rates at high pressures (30 atm.) and high temperatures (400°C.).

An unsuccessful attempt was made to operate the apparatus with a burette of steel instead of glass. The burette consisted of three bulbs formed by welding pairs of swaged nipples together. An electrical contact placed in the tubes above and below each bulb took the place of the scribe marks used with a glass burette. It was possible to calibrate the steel burette as accurately as the glass burette but the manipulation of the mercury level was difficult since one never knew how close the mercury was to a contact. The top contact was frequently overshot which forced mercury into the manifold and sometimes into the adsorbent chamber. Therefore the steel burette was removed and replaced by one of glass. The reason for trying to use a steel burette was that an adsorption isotherm could be obtained directly without the necessity of fitting adsorption and desorption runs together as was done in this investigation.

Results

The most serious problem in this investigation was in obtaining reproducible data. During the early runs it was found that even after reduction and evacuation for 500 hours at 400°C. the adsorption isotherms were not reproducible. The most successful procedure tried was to hold the catalyst at 550°C. for 8 hours and reduce it by flushing repeatedly with 500 psi. hydrogen followed by rough evacuation. In addition the catalyst was cleaned between runs by heating rapidly under vacuum to 400-500°C. and immediately cooling.

In taking the adsorption rate data there was always a question as to how long to continue one step before starting the next. That is, how closely must equilibrium be approached each time. In discussing the $\ln(p - p_\infty)$ versus time method (Experimental Data) for determining p_∞ it was pointed out that the final pressure obtained represented 97 per cent of equilibrium in most cases. The worst case in Runs 17 and 19 was Point 4 of Run 19 which was only within 85 per cent of equilibrium when the next point was started. This case can be investigated further using the results of the theoretical section. Substituting the data from Point 4 of Run 19 in Equation (16), which is the theoretical equation for the pressure-time data, gives

$$(p - p_\infty)/(p_1 - p_0) = 0.0157\, e^{-(0.000812)\theta} + 0.00204\, e^{-(0.00662)\theta} + \ldots$$

In order to determine p_∞, the last three points of Run 19, Point 4 were used, namely, 660, 750, and 1330 minutes. At 660 minutes the ratio of the second term in the above series to the first term is 1:355. Thus the one-term approximation

$$\ln(p - p_\infty) = \ln(0.0157)(p_1 - p_0) - (0.000812)\theta$$

is perfectly satisfactory in this case even though the adsorption was only 85 per cent complete. It is concluded, therefore, that the one-term approximation of Equation (16) and the time allowed to approach equilibrium were satisfactory in all the cases investigated.

The excellent agreement of the hydrogen equilibrium adsorption constant obtained in this investigation with the constant obtained by Pursley (28) in catalytic hydrogenation studies was surprising, particularly in view of the discussion in the introduction. This might be partially

explained by the fact that the equilibrium adsorption constant was nearly constant in the high-pressure region where this study overlapped the kinetic investigation.

The catalyst surface area of 19.5 $m.^2/gm.$ obtained from the Langmuir isotherm is considerably less than the 70 $m.^2/gm.$ obtained by the manufacturer (23) using the B.E.T. method. Although areas determined from the Langmuir isotherm are known to be quite inconsistent (10, chapter IV) one would expect these irregularities to be minimized at the high pressures attained in this study where the catalyst surface coverage is nearly complete. Perhaps the severe reduction procedure employed accounts for the decreased catalyst area.

The pressure variation of the f plot (Fig. 10) and the (V_pD/WL^2) plot (Fig. 11) is difficult to explain. Probably it is due to the fact that the dividing line between macropores and micropores is somewhat arbitrary and changes with pressure. It is believed that both of these plots would be better defined if adsorption studies were carried out using much smaller increments of gas than were used in this study. In addition the slope of the adsorption isotherm, (dn/dp), would be essentially constant so that E would be the same in both Equations (20) and (23). Then V_p could be found by solving Equations (20) and (23) simultaneously, and using this value of V_p in either equation one could find (D/L^2).

It is interesting to note the relationship of the term (V_pD/WL^2) to the Thiele modulus which was discussed in the introduction. Substituting $V_p = (1 - f)Ar$ in (V_pD/WL^2) yields

$$(V_pD/WL^2) = \left[(1 - f)A/W\right] (rD/L^2) \quad .$$

The ratio of the first-order reaction velocity constant C to the term (rD/L^2) in the above equation is $L^2(C/rD)$ which is the square of the Thiele modulus. If f were zero the term (rD/L^2) would refer to the entire catalyst pore system and rate of adsorption studies could be used to determine this portion of the Thiele modulus. Unfortunately, in the present case the term (rD/L^2) refers to the micropores which probably do not take part in any catalytic process.

CONCLUSIONS

The following conclusions may be drawn from this investigation of the adsorption of hydrogen on a nickel-kieselguhr catalyst at pressures up to 30 atm. from 0°C. to 300°C.:

1. Langmuir-type isotherms represent the data above one atm.

2. The adsorption equilibrium constant above one atm. is about 1.5 atm.$^{-1}$ at 200°C. and 0.75 atm.$^{-1}$ at 300°C. These values agree with the constant found in the same pressure and temperature range by Pursley (28) in his kinetic hydrogenation study.

3. The catalyst area is 19.5 m.^{2}/gm. The porosity is 51 per cent and the pore volume is 0.206 cc./gm.

4. The catalyst structure consists of macropores with an average diameter of 850 Å and micropores with an average diameter of approximately 10 Å. The micropores contain about 50 per cent of the catalyst area and 1 to 2 per cent of the pore volume.

5. Catalyst reduction at 30 atm. after a normal reduction at 1-3 atm. increases the surface area about 25 per cent. This increase occurs principally in the micropores.

6. The transient phenomenon which occurs whenever gas is admitted to or withdrawn from the catalyst is due to diffusion in the micropores.

7. The diffusion in the micropores is probably Knudsen-type with a correction for time-lag due to the average life of a molecule in the adsorbed state.

8. If the flow mechanism in small pores is effusion between "microchambers" instead of Knudsen-type diffusion in cylindrical pores, then the Knudsen diffusivity should be reduced by the factor $(d_o/d)^2$ where d is the average diameter of the equivalent cylindrical pores and d_o is the average diameter of the orifices between the "microchambers".

APPENDIX I

CALIBRATION OF EQUIPMENT

CALIBRATION OF EQUIPMENT

The determination of adsorption isotherms from volumetric adsorption equipment requires precise pressure, volume, and temperature measurements. In this section the calibrations and corrections which were necessary to provide these measurements will be discussed.

Temperature

In the following calibrations the primary standard thermometers, the zinc freezing point, and the Mueller bridge were corrected by means of National Bureau of Standard certificates.

Water Bath Thermometer: The thermometer to be calibrated was placed in a water bath which was adjusted to various temperatures in the vicinity of 25°C. Two platinum resistance thermometers were placed in the water bath and read with a Mueller bridge. From the calibration curve shown in Fig. 12 one sees that 25.00°C. corresponds to a thermometer reading of 24.823°C.

Thermocouple: An attempt was made to calibrate the thermocouple in place by installing an oil bath constructed from four pieces of pipe connected in the form of a square. One leg of this oil bath was placed around the thermocouple and a stirring motor and standard thermometer were placed in the opposite leg. All four sections of the oil bath were wrapped with electrical heating coils and covered with one inch of insulation but temperature gradients in the oil were never completely eliminated. Therefore this procedure was abandoned.

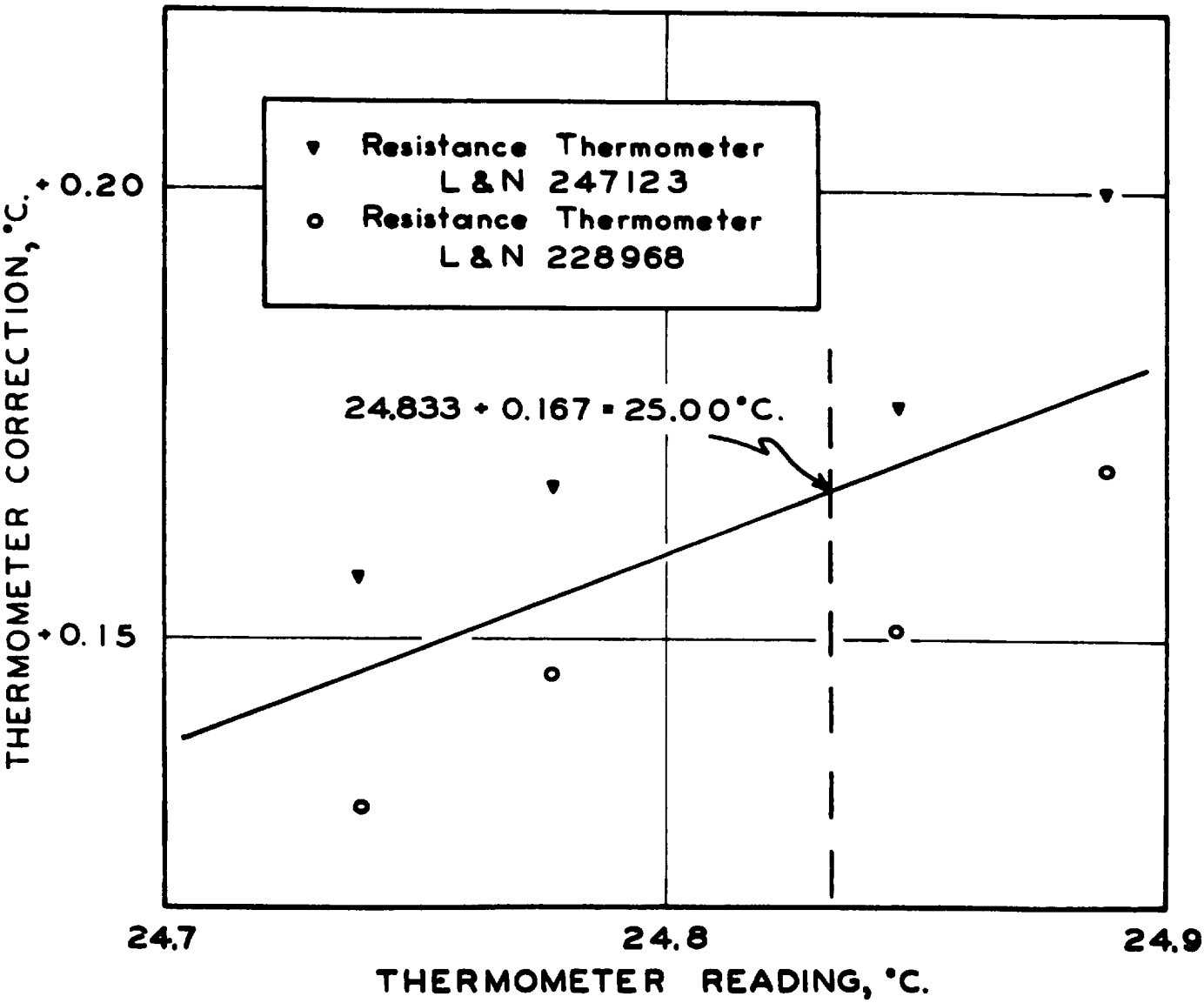

FIG. 12 WATER BATH THERMOMETER CALIBRATION CURVE

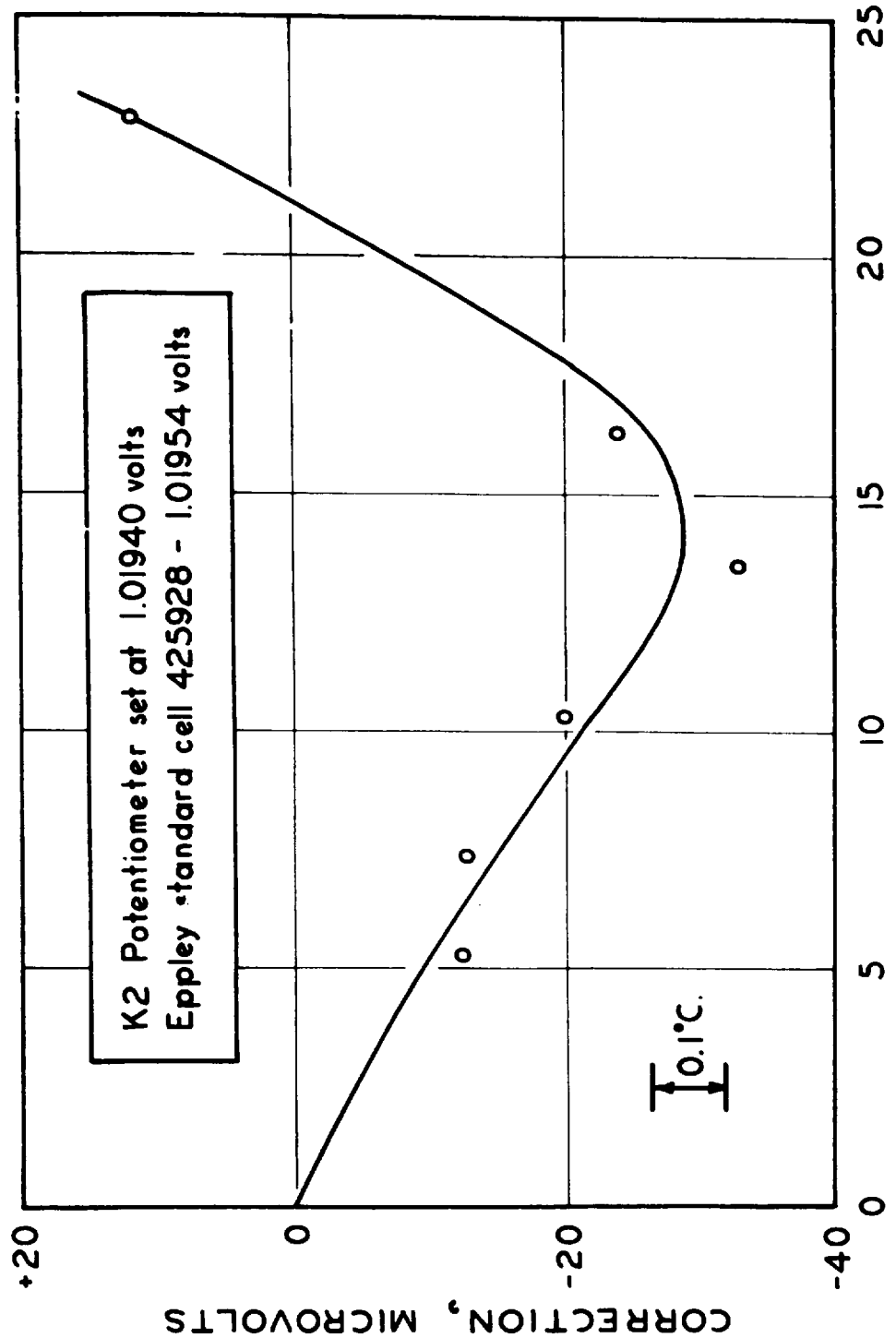

FIG. 13 IRON-CONSTANTAN THERMOCOUPLE CALIBRATION CURVE

The thermocouple was withdrawn from the thermocouple well, swung free of the equipment, and immersed in a small Dewar flask filled with Dow Corning silicone fluid, DC703. Temperatures up to 300°C. were measured with a standard thermometer. The oil bath was agitated with a stirring motor and heated with a small soldering iron connected to the Variac. In addition a furnace was placed around the thermocouple and a zinc freezing point determination made. The results are presented in Fig. 13 and Table 3.

TABLE 3

IRON-CONSTANTAN THERMOCOUPLE CALIBRATION

Temperature	Potentiometer Reading
0.0°C.	0 mv.
100.0	5.290
200.0	10.803
300.0	16.321
400.0	21.816

Pressure

Of the many pressure-measuring devices in the apparatus, precise readings are required from only the mercury manometer and the dead weight tester. Both of these are absolute measuring instruments and need no calibration but there are corrections to be made. For example, both are affected by the acceleration of gravity. An estimate of the local acceleration of gravity gave a correction factor of $g/g_c = 980.282/980.665$.

Manometer: The density of the mercury in the manometer must be corrected for the water bath temperature and the length of the brass scale of the cathetometer must be corrected to room temperature. The

...rections may be combined to give

$$p = \Delta h/763.4 \text{ atm.}$$

Dead Weight Tester: The dead weight tester operates through a mercury leg into the system. Correction for this mercury leg is determined by comparing the DWT and the mercury manometer readings for the pressure in the system with atmospheric pressure on the manometer. Therefore the true pressure is the sum of the manometer and barometric pressures. The absolute pressure of the dead weight tester was found to be

$$p = (DWT - 0.2)/14.702 \text{ atm.}$$

Compressibility: In making PVT calculations the ideal gas law was corrected for the compressibility of a real gas by the factor $z = pV/nRT$. The compressibility of hydrogen and helium was found to be linear with pressure in the temperature and pressure range of this experiment. Table 4 was prepared by means of data obtained from references (13), (35), and (36).

TABLE 4

COMPRESSIBILITY OF HYDROGEN AND HELIUM

T, °C.	1000(z-1)/p	
	Hydrogen	Helium
0	0.630	0.521
25	0.600	0.472
100	0.512	0.369
[illegible]	0.404	0.276
[illegible]00	0.334	.....
400	0.284	0.182

Volume

The volumes which must be calibrated are the burette, designated by 1, 2, 3, and 4; the space between the burette; the burette valve and the mercury in the manometer, designated by O; the manifold, M, connecting the burette section to the adsorbent chamber; and the free space in the loaded adsorbent chamber, C, including adsorbent pore volume. The procedure was to calibrate the burette volume first and then measure the remaining spaces in terms of the burette volume.

Burette: The burette bulbs were calibrated by draining the mercury from them and weighing it on Cenco scales which had a 2500-gm. capacity and an accuracy of 0.01 gm. Before starting a run some mercury was drawn off and releveled to the top burette scribe mark so that the mercury in the calibrating line external to the water bath would be at 25°C. After draining the desired number of burette bulbs the mercury was carefully leveled with the adjusting screw and a correction made for amount of screw rotation required. The results are shown in Table 5.

Secondary Volumes: The volume to be calibrated was connected to the burette section and the system filled with helium. Using this fixed quantity of gas the mercury was lowered one burette bulb at a time and the resulting pressure measured on the manometer. The slope of the plot PV/z versus P/z is the desired volume. It was calculated by the method of least squares. Table 6 presents a summary of the volume calibrations in terms of V/T where T is 298.16°K. This is the form in which it will be used later in the calculations.

TABLE 5

CALIBRATION OF THE BURETTE VOLUME

Burette Bulbs	Volume cc.	Average cc.
1	70.140 70.139 70.141 70.139	70.140
2	222.294 222.285 222.282 222.290 222.283 222.288	222.287
3	587.648 587.636 587.659 587.653 587.646 587.629	587.645
4*	806.053 806.054 806.059	806.055

* Calibration of the fourth burette bulb did not include the previous volumes.

TABLE 6

SUMMARY OF VOLUME CALIBRATIONS

V	V/T
0	0.08653 cc./°K.
1	0.32178
2	0.83209
3	2.0574
4	4.7609
M	0.02011
C	0.67133 (0°C)

Catalyst Free Space: Since the adsorbent chamber (249.22 cc. at 0°C.) is to be operated at various temperatures it is necessary to correct for the expansion of the chamber. In addition the tube (1.98 cc.) connecting the adsorbent chamber to the manifold will vary in temperature from one end to the other. The chamber expansion was calculated theoretically and combined with measurements of the catalyst free space at various temperatures to obtain the correction factors shown in Table 7.

TABLE 7

CATALYST FREE SPACE CORRECTIONS

T	(V/T) Correction
0°C.	0.00664 cc./°K.
100	0.00980
200	0.01154
300	0.01193

To use Table 7 first subtract the 0°C. correction from the catalyst free space V/T. Then compute the catalyst free space V/T at the temperatures desired and add the corrections. Table 8 shows the results for the catalyst used in the present experiment.

TABLE 8

CATALYST FREE SPACE

T	(V/T) Uncorrected	(V/T) Correction	(V/T) Corrected
0°C.	0.66469	0.00664	0.67133
100	0.48657	0.00980	0.49637
200	0.38372	0.01154	0.39526
300	0.31678	0.01193	0.32871

APPENDIX II

EXPERIMENTAL DATA

TABLE 9

EXPERIMENTAL PRESSURE-TIME DATA

Run 15.2

p mm.	θ min.
126.93	4
119.01	5
109.68	7
102.61	9
95.46	12
90.27	15
83.98	20
75.76	30
70.20	40
62.96	60
58.41	90
51.49	124
48.15	158
45.96	186
44.42	212
43.22	240

Run 15.4

p mm.	θ min.
548.83	3
541.46	5
535.91	7
531.07	9
525.51	12
520.61	15
514.00	20
501.83	32
491.98	45
483.91	60
467.32	96
459.52	120
448.99	162
400.21	620
396.99	683
394.17	741
392.47	790

Run 17.2

p mm.	θ min.
196.18	3
192.68	4
189.40	5
186.25	6
181.90	8
176.86	12
174.06	15
171.33	20
168.66	25
166.71	31
158.56	60
154.73	80
153.20	102
149.15	122
144.10	184
140.32	240
138.33	282

Run 17.4

p mm.	θ min.
598.21	2
594.90	3
592.37	4
590.32	5
588.59	6
586.78	7
585.27	8
582.98	10
580.97	12
578.37	15
575.10	20
572.20	25
569.24	31
564.92	42
560.50	55
556.38	70

Run 17.4 (cont)

p mm.	θ min.
547.14	110
540.89	150
539.56	240
524.93	300
518.35	360
508.36	500

Run 17.6

p psig.	θ min.
297.1	2
297.4	3
297.5	4
297.6	5
297.7	5.7
297.8	6.8
297.9	8.5
298.0	10
298.1	11.2
298.0	15
298.1	20
298.0	23
297.9	25
297.7	30
297.8	34

TABLE 9 (cont)

Run 17.8	
p psig.	θ min.
151.7	2.3
151.9	3
152.4	5.2
152.5	6
152.6	7
152.8	9.7
152.9	11.5
153.0	13
153.2	15
153.3	16.2
153.4	20
153.5	22
153.7	27
153.8	33
153.9	36
154.0	38
154.1	50
154.2	57
154.3	77

Run 17.10	
p psig.	θ min.
49.6	1.5
49.9	2
50.5	3
50.8	3.8
51.0	4.5
51.2	5.3
51.3	5.8
51.5	6.8
51.6	7.5
51.7	8
51.8	8.5
51.9	9.5
52.0	10.5
52.1	11.7
52.2	12.2
52.3	13.5
52.5	15.7

Run 17.10 (cont)	
p psig.	θ min.
52.6	17
52.7	19
52.8	20
52.9	22.5
53.1	24.7
53.3	29
53.6	35
53.7	46
53.5	60
54.0	65
54.4	67
54.0	78
54.2	90
54.4	115
55.4	157
55.3	170

Run 17.12	
p mm.	θ min.
409.92	3
414.06	4
417.09	5
419.19	6
423.56	8
427.13	10
430.16	12
433.05	16
438.01	23
442.94	34
448.44	52
452.05	70
456.64	115
463.76	212
466.19	270
470.54	315
470.54	345
471.95	390
477.37	1020

Run 18.2	
p mm.	θ min.
49.97	3
43.66	4
41.47	5
34.79	7
32.94	8
27.75	9
24.85	11
22.95	13
19.80	18
17.08	25
14.91	34
13.12	47
14.17	60
12.42	63
9.82	91
8.42	120
7.78	154
6.90	196
6.51	205
6.20	224

TABLE 9 (cont)

Run 18.4

p mm.	θ min.
499.37	3
492.38	4
486.10	5
481.07	6
476.71	7
472.60	8
469.00	9
465.82	10
457.74	13
452.99	15
443.22	20
428.97	30
409.82	50
395.67	72
375.68	120
359.71	180
340.15	301
337.80	320
336.71	330
330.45	390
325.29	450
321.92	496
292.05	1200

Run 18.6

p mm.	θ min.
483.16	1.5
481.71	2.5
480.45	3.5
479.56	4.5
478.38	6
477.18	8
476.03	10
475.02	12
473.94	15
472.18	20
469.23	30
464.42	50
459.44	75

Run 19.2

p mm.	θ min.
342.48	2
334.16	3
328.30	4
323.92	5
320.28	6
313.92	8
309.72	10
306.09	12
301.71	15
294.83	21
288.02	30
281.69	41
274.80	65
265.23	90
261.52	105
258.68	120
253.83	150
249.72	180
243.36	240
238.08	301
233.85	360
231.85	390
228.07	460
224.10	540
222.87	570
217.18	720
201.15	1380

Run 19.4

p mm.	θ min.
631.25	2
629.27	3
628.03	4
626.96	5
626.02	6
624.02	9
622.49	12
621.11	15
619.10	21

Run 19.4 (cont)

p mm.	θ min.
616.66	30
610.61	60
601.40	125
595.25	180
589.77	240
585.79	300
581.64	360
577.83	420
570.61	550
568.37	600
565.09	660
561.62	750
542.60	1330

Run 19.6

p mm.	θ min.
720.03	2
719.51	3
719.24	4.1
718.97	5
718.68	6
718.47	7
718.28	8.2
718.12	9.1
717.96	10
717.79	12
717.51	15
717.00	20.1

TABLE 9 (cont)

Run 19.12

P psig.	θ min.
163.3	3
163.9	4
164.5	5
164.6	[illegible]
[illegible]	[illegible]
[illegible]	[illegible]
[illegible]	[illegible]
165.7	10
166.0	12
166.3	15
[illegible]	[illegible]
[illegible]	[illegible]
167.5	55
167.7	[illegible]
[illegible]	[illegible]

Run 19.1[illegible]

P psig.	θ min.
[illegible]	[illegible]
[illegible]	3
[illegible]	[illegible]
[illegible]	[illegible]
[illegible]	6
[illegible]	[illegible]
[illegible]	[illegible]
[illegible]	[illegible]
[illegible]	[illegible]
[illegible]	17
[illegible]	30
[illegible]	60
60.2	790

Run 19.16

P mm.	θ min.
400.54	[illegible]
411.39	4.3
413.66	5.5
415.07	6.[illegible]

Run 19.16 (cont)

P mm.	θ min.
416.00	8
419.[illegible]	10
419.62	12
421.14	15
424.10	18
426.97	40
428.11	48
431.83	76
432.35	90
436.7[illegible]	1[illegible]
440.[illegible]	170
443.68	240
445.56	300
446.58	360
448.86	450
457.4[illegible]	1210

Run 20.[illegible]

P mm.	θ min.
64.82	3
56.1[illegible]	4
5[illegible].47	[illegible]
49.79	6
43.23	[illegible]
40.58	8
[illegible]	[illegible]
36.41	10
33.54	12
30.03	15
26.43	20
21.90	31
15.92	65
13.53	98
9.36	170
9.66	210
9.12	240
8.76	270

Run 20.4

P mm.	θ min.
495.15	2
484.80	3
477.18	4
471.44	5
466.13	6
461.53	7
457.47	8
450.3[illegible]	10
444.[illegible]	12
427.37	20
411.91	30
383.74	60
354.37	120
316.95	280
310.01	330
306.59	360
300.46	420
268.95	1[illegible]0
264.22	1085
263.47	1115
262.35	1150
261.88	1175

TABLE 9 (cont)

Run 26.2

p mm.	θ min.
730.36	2
731.33	3.2
732.17	4.5
732.66	5.8
733.02	6.2
733.26	8.4
733.37	9.8
733.58	10.8
733.75	12.2
734.00	15
734.19	18
734.42	23
734.60	30
734.80	46
735.10	65
735.15	95
735.48	128
735.50	154
735.57	180
735.76	240
735.95	300
736.10	360
735.97	420
736.08	430
736.18	480
736.16	570
736.16	600

TABLE 10

DATA SUMMARY

Point	V	θ min.	P_θ	P_1	$1000xS_1$ $min.^{-1/2}$	P_2	P_∞	$-1000xS_\infty$ $min.^{-1}$
Run 15 - Hydrogen - 0°C.								
1	4 MC		751.59 mm. 0					
2	4MC	240	43.22 mm.	168 mm.	131	...	38 mm.	8.04
3	4M		726.00 mm.					
4	4MC	790	392.47 mm.	571.9 mm.	25.5	...	376 mm.	2.23
Run 18 - Hydrogen - 0°C.								
1	4 MC		750.15 mm. 0					
2	4MC	224	6.20 mm.	76 mm.	205	16.0 mm.	5.05 mm.	10.0
3	4M		768.06 mm.					
4	4MC	1200	292.05 mm.	544.1 mm.	47.9	379 mm.	279 mm.	1.70
5	2M		727.90 mm.					
6	2MC	75	459.44 mm.	488.33 mm.	20.09			

TABLE 10 (cont)

Point	V	θ min.	p_θ	p_1	$1000xS_1$ $min.^{-1/2}$	p_2	p_∞	$-1000xS_\infty$ $min.^{-1}$
Run 17 - Hydrogen - 200°C.								
1	4		742.47 mm.					
	MC		0					
2	4MC	282	138.33 mm.	218.6 mm.	59.38	167.1 mm.	130.8 mm.	5.577
3	4M		765.71 mm.					
4	4MC	500	508.36 mm.	609.8 mm.	18.08	561.9 mm.	477.8 mm.	2.022
5	0		460.62 mm.					
	MC		462.1 psig.					
6	4		755.96 mm.					
	MC	34	297.8 psig.	296.5 psig.	3.02	...	297.8 psig.	...
7	0		457.84 mm.					
8	4		700.09 mm.					
	MC	77	154.3 psig.	150.2 psig.	6.48	151.9 psig.	154.3 psig.	53.6
9	0		462.83 mm.					
10	4		561.40 mm.					
	MC	170	55.3 psig.	47.4 psig.	16.6	52.9 psig.	58 psig.	2.4
11	0		460.10 mm.					
12	4MC	1020	477.37 mm.	392.2 mm.	4.235	441.37 mm.	477.59 mm.	5.128

TABLE 10 (cont)

Point	V	θ min.	p_θ	p_1	$1000xS_1$ $min.^{-1/2}$	p_2	p_∞	$-1000xS_\infty$ $min.^{-1}$
Run 19 - Hydrogen - 300°C.								
1	4		742.32 mm.					
	MC		0					
2	4MC	1380	201.15 mm.	380 mm.	70	255.7 mm.	186.7 mm.	1.136
3	4M		763.84 mm.					
4	4MC	1330	542.60 mm.	637.3 mm.	10.3	604.1 mm.	10.6 mm.	0.810
5	4M		760.39 mm.					
6	4MC	20.1	717.02 mm.	721.4 mm.	5.21			
11	0		463.63 mm.					
	MC		456.0 psig.					
12	4		451.38 mm. + 734.2 mm. barometer					
	MC	120	167.7 psig.	159.9 psig.	6.68	164.7 psig.	167.7 psig.	46.1
13	0		459.28 mm.					
14	4		562.09 mm.					
	MC	790	60.2 psig.	48.0 psig.	18.3	55.7 psig.	60.2 psig.	11
15	OM		513.59 mm.					
16	4MC	1210	457.49 mm.	394.1 mm.	3.06	439 mm.	466 mm.	0.982

TABLE 10 (cont)

Point	V	θ min.	p_θ	p_1	$1000xS_1$ min.$^{-1/2}$	p_2	p_∞	$-1000xS_\infty$ min.$^{-1}$
Run 20 - Hydrogen - 0°C.								
1	4		759.98 mm.					
	MC		0					
2	4MC	270	8.76 mm.	103 mm.	215	20.5 mm.	7.4 mm.	8.55
3	4M		748.41 mm.					
4	4MC	1175	261.88 mm.	541 mm.	61.0	360 mm.	249 mm.	1.82
Run 26 - Helium - 0°C.								
1	0		Vent open for 20 seconds while pressure in MC dropped to 1 atm.					
	MC		507.3 psig.					
2	OMC	600	736.16 mm.	726.7 mm.	0.119	734.4 mm.	736.2 mm.	6.0

APPENDIX III

DATA PROCESSING

DATA PROCESSING

Isotherms

The construction of an adsorption isotherm consists of adding up the amounts of gas that are adsorbed (or desorbed) each time a quantity of gas is admitted to (or withdrawn from) the adsorbent chamber. The amount of gas adsorbed is determined from the difference in the amount of material present in the burette and adsorbent chamber before and after admitting gas to the catalyst. These quantities can be calculated from the data in Table 10 using the information in Appendix I. Table 11 is an example of such calculations.

To calculate the first point on the adsorption isotherm one notes from Table 11 that nR = 4.681 initially for the burette and zero for the adsorbent chamber (point 1). At equilibrium (point 2) nR = 0.036 for both the burette and the adsorbent chamber, giving an adsorption of nR = 4.645, which is recorded in Table 12. Since equilibrium was not reached before the first step was stopped, the amount of gas actually adsorbed at the final pressure reached, p_θ, is nR = 4.637. The second quantity of gas adsorbed must be added to nR = 4.637 rather than nR = 4.645.

For the second step nR = 4.809 + 0.005 initially for the burette and adsorbent chamber and nR = 1.992 at equilibrium. This represents an adsorption of nR = 2.822 which added to the previous value of nR = 4.637 is nR = 7.459.

TABLE 11

SAMPLE CALCULATIONS. RUN 18 (0°C.)

Point	V	p atm.	p/z atm.	V/T cc./°K.	nR atm.–cc./°K.
$1p_B$	4	0.9834	0.9828	4.7609	4.681
$2p_1$	4MC	0.0996	0.0996	5.4523	0.543
$2p_\theta$	4MC	0.0081	0.0081	5.4523	0.044
$2p_\infty$	4MC	0.0066	0.0066	5.4523	0.036
$2p_\theta$	C	0.0081	0.0081	0.6713	0.005
$3p_B$	4M	1.0061	1.0055	4.7810	4.809
$4p_1$	4MC	0.7126	0.7123	5.4523	3.882
$4p_\theta$	4MC	0.3829	0.3828	5.4523	2.085
$4p_\infty$	4MC	0.3658	0.3657	5.4523	1.992
$4p_\theta$	C	0.3829	0.3828	0.6713	0.257
$5p_B$	2M	0.9538	0.9533	0.85220	0.812
$6p_1$	2MC	0.6400	0.6398	1.5235	0.974

TABLE 12

SUMMARY OF SAMPLE CALCULATIONS. RUN 18 (0°C.)

Point	p_∞ atm.	nR	
		p_θ	p_∞
..	0		0
2	0.0066	4.637	4.645
4	0.3658		7.459

In Runs 17 and 19 the desorption portion of the isotherm is calculated in a similar fashion and the adsorption and desorption portions of the run fitted together graphically. Dividing the values of nR by W (W = 370.39 gm.) gives the data for Table 13. Table 11 includes information at p_1 used in preparing the f chart.

Diffusion

Tables 15, 16, and 17 show the procedure used to calculate V_1D/L^2 from Equations (20) and (23). The slope of the adsorption isotherm, (dn/dp), required to calculate E was determined by measuring the slope of n versus ln p graphically and dividing by p. A value of f = 0.5 was used throughout. There is further discussion of these calculations in the section on experimental and theoretical results.

TABLE 13

HYDROGEN ADSORPTION ISOTHERMS ON NICKEL-KIESELGUHR

Run	p atm.	$nx10^4$ moles/gm.	$(p/n)x10^{-4}$ atm.-gm./mole
15 (0°C.)	0	0	.....
	0.0498	1.468	0.034
	0.4927	2.082	0.327
17 (200°C.)	0	0	.....
	0.1714	1.232	0.139
	0.6260	1.767	0.354
	0.6259	1.767	0.354
	3.932	2.279	1.725
	10.49	2.522	4.159
	20.23	2.629	7.70
	31.41	2.663	11.79
18 (0°C.)	0	0	.....
	0.0066	1.528	0.0043
	0.3658	2.452	0.149
19 (300°C.)	0	0	.....
	0.2448	1.111	0.220
	0.6694	1.556	0.430
	0.6104	1.516	0.403
	4.082	2.078	1.965
	11.40	2.378	4.798
	30.99	2.582	11.99
20 (0°C.)	0	0	.....
	0.0097	1.541	0.0063
	0.3263	2.327	0.140

TABLE 14

FRACTION OF CATALYST SURFACE READILY ACCESSIBLE

Run	p_1 atm.	f
17 (200°C.)	0.2863	0.71
	0.7988	0.26
	0.5141	0.55
	3.211	0.49
	10.21	0.61
	20.17	0.43
18 (0°C.)	0.0996	0.62
	0.7126	0.30
	0.6400	0.33
19 (300°C.)	0.4980	0.48
	0.8345	0.38
	0.9450	0.42
	0.5163	0.64
	3.251	0.57
	10.87	0.66
20 (0°C.)	0.1350	0.57
	0.7093	0.25

TABLE 15

CALCULATION OF (V_pD/L^2) FROM INITIAL SLOPES

$(p_0+p_1)/2$ atm.	$\bar{V}/T$ cc./°K.	(1-f)E	(1+fE)	$1000S_1$ min.$^{-1/2}$	$(\pi/4)\bar{V}S_1^2$ cc./min.	V_pD/L^2 cc./min.
Run 17 (200°C.)						
0.143	5.176	1.49	1.44	59.38	6.79	9.45
0.486	5.176	0.293	1.13	18.08	0.629	2.74
2.223	5.176	0.0506	1.22	4.235	0.0346	1.02
6.85	0.4154	0.149	1.28	16.6	0.0426	0.468
15.22	0.4154	0.0408	1.07	6.48	0.00650	0.182
25.79	0.4154	0.0225	1.03	3.02	0.00141	0.0665
Run 18 (0°C.)						
0.050	5.452	6.15	1.62	205	49.1	21.0
0.360	5.452	0.410	1.08	47.9	2.68	7.64
0.503	1.524	0.347	1.31	20.09	0.132	0.651
Run 19 (300°C.)						
0.249	5.110	0.855	1.25	70	11.3	20.6
0.540	5.110	0.267	1.13	10.3	0.244	1.17
0.807	5.110	0.142	1.12	5.21	0.0624	0.551
2.299	5.110	0.0524	1.24	3.06	0.0216	0.635
7.325	0.3488	0.194	1.36	18.3	0.0526	0.501
20.93	0.3488	0.0471	1.10	6.68	0.00700	0.180
Run 20 (0°C.)						
0.0675	5.452	4.77	1.51	215	54.1	25.9
0.360	5.452	0.443	1.07	61.0	4.35	11.2
Run 26						
17.49	0.7780	0	1	0.119	2.37×10^{-6}	....

TABLE 16

CALCULATION OF (V_pD/L^2) FROM FINAL SLOPES

P_∞ atm.	$\bar{V}/T$ cc./°K.	(1-f)E	β_1	$-1000S_\infty$ min.$^{-1}$	$-\bar{V}S_\infty/\beta_1^2$ cc./min.	V_pD/L^2 cc./min.
Run 17 (200°C.)						
0.1714	5.176	0.784	1.81	5.577	4.16	3.26
0.6260	5.176	0.173	1.66	2.022	1.80	0.312
0.6259	5.176	0.173	1.66	5.128	4.55	0.787
3.932	0.4154	0.217	1.68	2.4	0.167	0.0362
10.49	0.4154	0.0657	1.61	53.6	4.08	0.268
Run 18 (0°C.)						
0.0066	5.452	11.0	2.00	10.0	3.72	40.9
0.3658	5.452	0.139	1.64	1.70	0.942	0.131
Run 19 (300°C.)						
0.2448	5.110	0.580	1.78	1.136	1.050	0.608
0.6694	5.110	0.179	1.66	0.810	0.861	0.154
0.6104	5.110	0.197	1.67	0.982	1.032	0.203
4.082	0.3488	0.275	1.70	11	0.761	0.209
11.40	0.3488	0.0882	1.62	46.1	3.517	0.310
Run 20 (0°C.)						
0.0097	5.452	9.13	2.00	8.55	3.18	29.0
0.3263	5.452	0.184	1.66	1.82	0.984	0.181
Run 26 (0°C.)						
0.965	0.7780	0	1.57	6.0	0.519	.....

TABLE 17

SUMMARY OF (V_pD/L^2) CALCULATIONS

Calculated from Initial Slope		Calculated from Final Slope	
$(p_0+p_1)/2$ atm.	$(V_pD/WL^2)\times10^5$ cc./gm.-sec.	p_∞ atm.	$(V_pD/WL^2)\times10^5$ cc./gm.-sec.
Run 17 (200°C.)			
0.143	42.5	0.1714	14.66
0.486	12.3	0.6260	1.40
2.223	4.59	0.6259	3.54
6.85	2.10	3.932	0.163
15.22	0.819	10.49	1.21
25.79	0.299		
Run 18 (0°C.)			
0.050	94.5	0.0066	184
0.360	34.4	0.3658	0.590
0.503	2.93		
Run 19 (300°C.)			
0.249	92.7	0.2448	2.73
0.540	5.26	0.6694	0.693
0.807	2.48		
2.299	2.86	0.6104	0.913
7.325	2.25	4.082	0.940
20.93	0.810	11.40	1.39
Run 20 (0°C.)			
0.0675	116.5	0.0097	130.5
0.360	49.6	0.3263	0.814

APPENDIX IV

DERIVATIONS

THE LANGMUIR ADSORPTION ISOTHERM

When the molecules of a gas strike a surface they may either rebound elastically or they may stay in contact with the surface for a period of time before returning to the gas phase. According to Langmuir (21 and 22) this time lag is responsible for the phenomenon of adsorption. The derivation of the Langmuir adsorption isotherm is discussed briefly in the following paragraphs.

If v is the average molecular velocity and the molar concentration per unit volume is y then from the kinetic theory of gases the rate at which molecules strike a surface of unit area is vy/4; see for example Hennard (20). The rate of condensing on a surface is $\alpha vy/4$ where α is the condensation coefficient. If n' is the molar concentration of adsorbed molecules per unit area, the net rate of adsorption is

$$\frac{dn'}{d\theta} = \alpha vy/4 - k'n' \quad , \tag{33}$$

where k' is the average probability per second for the evaporation of molecule. The reciprocal of k' is τ, the average life of an adsorbed molecule.

According to Langmuir only those molecules striking bare surface will condense so that

$$\alpha = \alpha_0 \left[\frac{n_m' - n'}{n_m'} \right] \quad ,$$

since $(n_m' - n')/n_m'$ is the fraction of bare surface. Here, n_m' is the molar concentration of adsorbed molecules per unit area when the surface

completely covered and α_0 is a constant usually taken to be unity. Substituting this value of α into Equation (33) gives

$$\frac{dn'}{d\theta} = \frac{\alpha_0 v(n_m' - n')}{4 n_m'} y - k'n' \quad . \tag{34}$$

If n moles/gm. is the concentration of adsorbate on W grams of catalyst with a total surface area A then $An' = Wn$. Substituting $n_m' = n_m A$ and $y = p/RT$ in Equation (34) gives

$$\frac{dn'}{d\theta} = \frac{\alpha_0 vA(n_m' - n')}{4 RT W n_m} p - k'n' \quad .$$

In reaction kinetics (17, p. 910) it is customary to write the equation for the net rate of adsorption in the form

$$\frac{dn'}{d\theta} = k(n_m' - n') p - k'n' \quad ,$$

so that

$$k = \frac{\alpha_0 vA}{4 RT W n_m} \quad .$$

At equilibrium

$$\frac{dn'}{d\theta} = 0 \quad ,$$

and

$$K = \frac{k}{k'} = \frac{\alpha_0 vA}{4 RT W n_m k'} = \frac{n}{p(n_m - n)} \quad , \tag{35}$$

where K is the equilibrium adsorption constant. Equation (35) can be rearranged to give

$$n/n_m = \frac{K p}{1 + K p} \quad , \tag{1}$$

which is the Langmuir adsorption isotherm.

The desorption rate can be found by solving Equation (35) for k':

$$k' = \frac{\alpha_0 \, v \, A}{4 \, RT \, W \, n_m \, K} \quad .$$

If α_0 is taken as unity then all the remaining factors are known or can be found from the experimental data. An average value for K based on the upper end of the 200°C. isotherm is 1.5, taking $n_m = 2.7 \times 10^{-4}$ moles/gm. Therefore at 200°C.

$$k' = \frac{(2.23 \times 10^5)(19.5 \times 10^4)}{4(82.06)(473.2)(2.7 \times 10^{-4})(1.5)}$$

$$k' = 6.9 \times 10^8 \text{ sec.}^{-1} \quad .$$

Recalling that the reciprocal of k' is the average life of an adsorbed molecule one obtains

$$\tau = 1.4 \times 10^{-9} \text{ sec.} \quad .$$

at 200°C.

THE RATE OF ADSORPTION AT CONSTANT VOLUME

The net rate of adsorption on a surface as derived in Appendix IV, equation (34), is

$$\frac{dn'}{d\theta} = \frac{\alpha_0 \, v(n_m' - n')}{4 \, n_m'} y - k'n' \quad . \tag{34}$$

Since both n' and y are functions of time their product is a non-linear term which would be difficult to handle in the following derivation. If an average value is assumed for the molal number of unoccupied sites per unit area, $(n_m' - n')$, then as an approximation Equation (34) can be written

$$\frac{dn'}{d\theta} = k_0 y - k'n'(\theta) \quad . \tag{36}$$

If the initial value of $n'(\theta)$ is n_0' then

$$n'(\theta) = n_0' - \int_0^\theta \frac{dn'}{d\theta} \, d\theta \quad ,$$

$$n'(\theta) = n_0' - \int_0^\theta k_0 y(\theta) d\theta - \int_0^\theta k'n'(\theta) d\theta \quad . \tag{37}$$

The Laplace transform of Equation (37) is

$$n'(s) = n_0'/s - \frac{k_0 y(s) - k'n'(s)}{s} \quad ,$$

which can be solved for n'(s) to give

$$n'(s) = \frac{n_0' + k_0 y(s)}{s + k'} \quad . \tag{38}$$

The Laplace transform of a function $u(\theta)$ is defined here by

$$u(s) = \int_0^{\infty} e^{-s\theta} \, u(\theta) \, d\theta \quad .$$

If the concentration of gas within the pore structure of a catalyst is in equilibrium with the gas surrounding the catalyst; then during the time $d\theta$ the total accumulation,

$$(\bar{V} + V_p) \frac{dy}{d\theta} \quad ,$$

plus the total adsorption on W gms. of catalyst of area A,

$$A \frac{dn'}{d\theta} \quad ,$$

must be zero. From Equation (36)

$$V \frac{d}{d\theta} y(\theta) + Ak_0 y(\theta) - Ak'n'(\theta) = 0 \quad , \qquad (39)$$

where

$$V = \bar{V} + V_p \quad .$$

If $y(0) = y_0$ the Laplace transform of Equation (39) is

$$Vsy(s) - Vy_0 + Ak_0 y(s) - Ak'n'(s) = 0 \quad . \qquad (40)$$

Substituting Equation (38) in (40) gives after some rearranging

$$sy(s) = \frac{C_1 + y_0 s}{s + C_2} \quad , \qquad (41)$$

where

$$C_1 = y_0 k' + Ak'n_0'/V \quad ,$$

$$C_2 = k' + Ak_0/V \quad .$$

Equation (41) can be put in the form

$$y(s) = \frac{C_1}{s}\left[\frac{1}{s + C_2}\right] + y_0\left[\frac{1}{s + C_2}\right]. \qquad (42)$$

The inverse of Equation (42) is

$$y(\theta) = C_1 \int_0^{\theta} e^{-C_2\theta}\, d\theta + y_0 e^{-C_2\theta} ,$$

and

$$y(\theta) = C_1/C_2 + (y_0 - C_1/C_2)e^{-C_2\theta} .$$

But

$$y(\infty) = C_1/C_2 + 0 ,$$

so that

$$\left[\frac{y(\theta) - y_\infty}{y_0 - y_\infty}\right] = e^{-C_2\theta} . \qquad (43)$$

At equilibrium Equation (36) becomes

$$\frac{dn'}{d\theta} = k_0 y - k'n' = 0 ,$$

and

$$k_0 = k'n'/y .$$

Since An' = nW and y = p/RT

$$k_0 A/V = k'F ,$$

where

$$F = WnRT/R_\infty(\bar{V} + V_p) .$$

Thus

$$C_2 = k'(1 + F) ,$$

and Equation (43) becomes

$$\ln\left[\frac{P - P_{\infty}}{P_0' - P_{\infty}}\right] = - k'(1 + F)\theta \quad . \qquad (3)$$

DIFFUSION AND ADSORPTION IN CYLINDRICAL CATALYST PORES

In the theoretical section, Boundary Value Problem 15,

$$\left.\begin{aligned} D\frac{\partial^2}{\partial x^2}y(x,\theta) &= (1 + c/r)\frac{\partial}{\partial\theta}y(x,\theta) \\ y(x,0) &= y_0 \\ \frac{\partial}{\partial x}y(L,\theta) &= 0 \\ y(0,\theta) &= \bar{y}(\theta) \quad , \end{aligned}\right\} \tag{15}$$

was derived for the diffusion and adsorption of a gas in cylindrical catalyst pores. Substituting the following dimensionless equations,

$$\begin{aligned} z &= x/L \\ t &= D\theta/L^2(1 + c/r) \\ Y(z,t) &= \left[y(z,t) - y_0\right]/(\bar{y}_1 - y_0) \quad , \end{aligned} \tag{17}$$

and Equation (10) into Boundary Value Problem 15 yields

$$\left.\begin{aligned} \frac{\partial^2}{\partial z^2}Y(z,t) &= \frac{\partial}{\partial t}Y(z,t) \\ Y(z,0) &= 0 \\ \frac{\partial}{\partial z}Y(1,t) &= 0 \\ Y(0,t) &= 1 - B\,Y(t) \quad . \end{aligned}\right\} \tag{44}$$

A convenient tool for the solution of transient problems is the Laplace transformation (Churchill, 14). The Laplace transformation of

Y(z,t) is defined

$$U(z,s) = \int_0^\infty e^{-st}\, Y(z,t)dt \quad .$$

The boundary value problem in the transform U(z,s) becomes

$$\frac{\partial^2}{\partial z^2} U(z,s) = s\, U(z,s)$$

$$\frac{\partial}{\partial z} U(1,s) = 0$$

$$U(0,s) = 1/s - B\, U(s) \ ,$$

which can be solved by elementary methods to give

$$U(z,s) = \left[\frac{1/s - BU(s)}{e^{\sqrt{s}} + e^{-\sqrt{s}}}\right](e^{\sqrt{s}}\, e^{-\sqrt{s}\, z} + e^{-\sqrt{s}}\, e^{\sqrt{s}\, z}) \quad .$$

Since

$$U(s) = \frac{\int_0^1 U(z,s)dz}{\int_0^1 dz} \ ,$$

U(z,s) can be integrated over z to obtain

$$U(s) = \left[\frac{1/s - BU(s)}{e^{\sqrt{s}} + e^{-\sqrt{s}}}\right](e^{\sqrt{s}} - e^{-\sqrt{s}})/\sqrt{s} \ ,$$

and solved for U(s),

$$U(s) = \frac{1}{s(B + \sqrt{s}\ \mathrm{ctnh}\ \sqrt{s})} \quad . \qquad (45)$$

The inverse, Y(t), of U(s) is the required function describing the variation of the average micropore concentration with time. The general procedure for finding the inverse is to determine the poles of U(s) and to evaluate the residues of $e^{st}\, U(s)$ at these poles. U(s) has

simple pole at s = 0 since

$$\lim_{s\to 0} (B + \sqrt{s}\ \mathrm{ctnh}\ \sqrt{s}) = \lim_{s\to 0} (B + 1 + s^2/3 + \ldots) = (B + 1) .$$

The residue $e^{st}\ U(s)$ at s = 0 is therefore

$$1/(B + 1) .$$

The roots of

$$B + \sqrt{s}\ \mathrm{ctnh}\ \sqrt{s} = 0 ,$$

must be located to determine the remaining residues. For generality assume that

$$\sqrt{s} = \alpha + i\beta ,$$

where α and β are both real and not zero. Substituting for $\sqrt{s}$ and separating real and imaginary terms gives

$$B \sinh\alpha \cos\beta + \alpha \cosh\alpha \cos\beta - \beta \sinh\alpha \sin\beta = 0 ,$$

$$B \cosh\alpha \sin\beta + \beta \cosh\alpha \cos\beta + \alpha \sinh\alpha \sin\beta = 0 ,$$

which may be rearranged and combined to give

$$\sinh\alpha \cosh\alpha/\alpha = \sin\beta \cos\beta/\beta .$$

Except for $\alpha = \beta = 0$ there are no solutions to this equation since the term $(\sinh\alpha \cosh\alpha/\alpha)$ is greater than one for all $\alpha \neq 0$ and $(\sin\beta \cos\beta/\beta)$ is less than one for all $\beta \neq 0$. Therefore $\sqrt{s}$ is not complex. If β is assumed to be zero then

$$B + \alpha \operatorname{ctnh} \alpha = 0 ,$$

which has no solution since $\alpha \operatorname{ctnh} \alpha \geq 0$ for all α. Thus $\sqrt{s}$ must be imaginary. So

$$B + \beta_j \cot \beta_j = 0 ,$$

and

$$\tan \beta_j = - \beta_j / B = \eta .$$

The solutions of this equation are shown in Fig. 14.

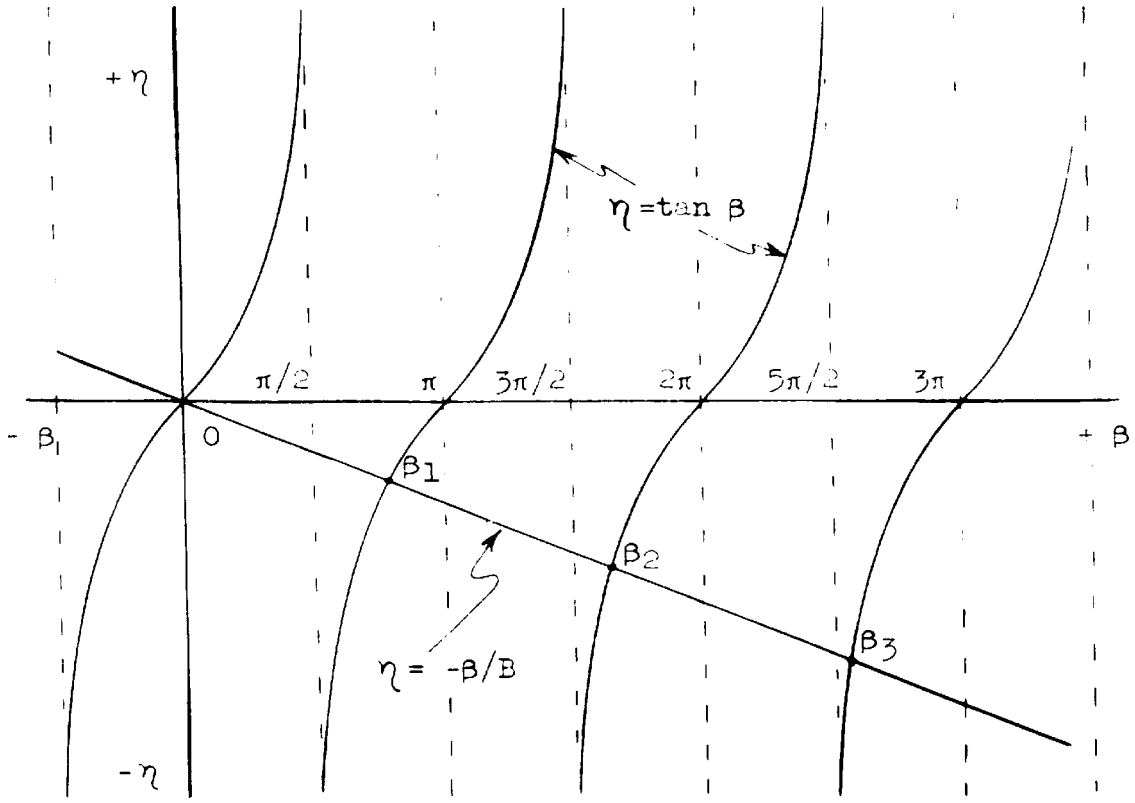

Fig. 14. Solutions of the Equation $B + \beta \cot \beta = 0$.

The sum of the residues at the poles $s_j = -\beta_j^2$ is

$$\sum_{j=1}^{j=\infty} \left[\frac{-2}{B + B^2 + \beta_j^2} \right] e^{-\beta_j^2 t} \quad .$$

The complete inverse transform is then

$$Y(t) = \frac{1}{B+1} - 2 \sum_{j=1}^{j=\infty} (B + B^2 + \beta_j^2)^{-1} e^{-\beta_j^2 t} \quad , \qquad (46)$$

where

$$\beta_j \cot \beta_j + B = 0 \quad . \qquad (18)$$

Although the problem is now solved the result is not in a useful form. Experimentally the variations in gas concentration external to the catalyst are observed rather than the average micropore concentration, Y(t). Recalling that

$$\bar{y}_1 - \bar{y}(t) = B \left[y(t) - y_0 \right] \quad , \qquad (10)$$

$\bar{Y}(t)$ is defined

$$\bar{Y}(t) = \left[\frac{\bar{y}_1 - \bar{y}(t)}{\bar{y}_1 - y_0} \right] = BY(t) \quad . \qquad (47)$$

Hence

$$\bar{Y}(t) = \frac{B}{B+1} - \sum_{j=1}^{j=\infty} \left[\frac{2B}{B + B^2 + \beta_j^2} \right] e^{-\beta_j^2 t} \quad ,$$

but

$$\bar{Y}(\infty) = \frac{B}{B+1} - 0$$

so that

$$\bar{Y}(\infty) - \bar{Y}(t) = \left[\frac{\bar{y}(t) - \bar{y}_0}{\bar{y}_1 - y_0}\right] = \sum_{j=1}^{j=\infty}\left[\frac{2B}{B + B^2 + \beta_j^2}\right] e^{-\beta_j^2 t} \quad ,$$

which describes the variation in the experimentally observed concentration, $\bar{y}(t)$, with time.

At small values of t the above series converges slowly so that it is difficult to evaluate. However, in the early stages of diffusion the change in concentration has not become appreciable at the end of the pores so the problem reduces to one of diffusion in semi-infinite pores. Liebhafsky (24) used this procedure to obtain a very simple approximation for the initial rate of diffusion. An alternate, and much simpler procedure is possible using the Laplace transformation if one remembers that small t corresponds to large s. Then the transform

$$U(s) = \frac{1}{s(B + \sqrt{s}\ \mathrm{ctnh}\ \sqrt{s})} \quad , \qquad (45)$$

reduces to the approximate equation

$$U(s) \doteq \frac{1}{s(B + \sqrt{s})} \quad ,$$

because

$$\lim_{s \to \infty} \mathrm{ctnh}\ \sqrt{s} = 1 \quad ,$$

and

$$U(s) \doteq s^{-3/2} - B\, s^{-2} + B\, s^{-5/2} + \ldots \quad ,$$

has the simple inverse

$$Y(t) \doteq 2(t/\pi)^{1/2} - Bt + \ldots \quad .$$

For small t

$$Y(t) \doteq 2(t/\pi)^{1/2} \quad .$$

Recalling that

$$\bar{Y}(t) = BY(t) \quad , \tag{47}$$

then

$$\bar{Y}(t) \doteq 2B(t/\pi)^{1/2} \quad .$$

The concentration variables can now be replaced by pressures using the substitution

$$y = \frac{n}{v} = \frac{p}{RT} \quad ,$$

where

$$p = RT\,\bar{y}(t)$$

$$p_0 = RT\,\bar{y}_0 = RT\,y_0$$

$$p_1 = RT\,\bar{y}_1$$

$$p_\infty = RT\,\bar{y}_\infty = RT\,y_\infty \quad .$$

Then

$$\left[\frac{p - p_\infty}{p_1 - p_0}\right] = \sum_{j=1}^{j=} \left[\frac{2B}{B + B^2 + \beta_j^2}\right] e^{-\beta_j^2 t} \quad , \tag{16}$$

and

$$\left[\frac{p_1 - p}{p_1 - p_0}\right] \doteq 2B(t/\pi)^{1/2} \quad . \tag{21}$$

It is possible to make an interesting reduction of this problem of adsorption at constant volume to the case of adsorption at constant pressure. If $\bar{V}$ is allowed to expand until it becomes an infinite reservoir, B becomes zero according to Equation (11) and operation is then at constant pressure. (Of course experimentally an infinite reservoir is not used to obtain constant pressure operation.) From Fig. 14 it is seen that as B approaches zero β_j approaches $(2j - 1)\pi/2$. Substituting

$$B = 0$$

$$\beta_j = (2j - 1)\pi/2 \quad ,$$

in Equation (46) gives

$$\left[\frac{y_\infty - y(t)}{y_\infty - y_0} \right] = \frac{8}{\pi^2} \sum_{j=1}^{j=\infty} (2j - 1)^{-2} \, e^{-(2j-1)^2\pi^2 t/4} \quad ,$$

which is the solution frequently mentioned in the literature (10, p. 462, and 12, p. 79) for the average concentration in a body undergoing one-dimensional diffusion from faces at fixed concentrations. The short-time solution is still

$$\left[\frac{y(t) - y_0}{y_\infty - y_0} \right] = 2(t/\pi)^{1/2} \quad .$$

Both of these solutions may be readily related to the experimentally observed volume changes taking place at constant pressure.

EFFUSION AND ADSORPTION IN A POROUS CATALYST

Except for the change in geometry the assumptions and general procedure used previously for studying diffusion in cylindrical pores will be followed. Assume that the micropore structure of a catalyst consists of N rows of chambers with an average of J connecting chambers in a row and that the NJ chambers have a total volume V_p, an average hydraulic radius r, and a total surface area V_p/r. Let the hydraulic radius of the orifice between chambers be r_o.

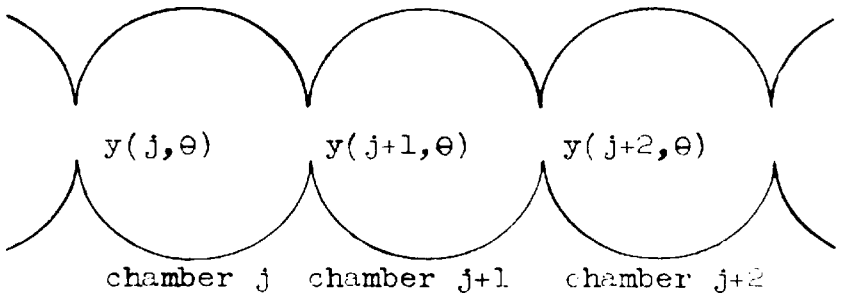

Fig. 15. Micropore consisting of a series of connecting chambers.

The passage of gas through a small orifice in a thin wall is given by

$$\text{Rate of Effusion} = \pi r_o^2 v y \quad ,$$

when the mean free path is large in comparison with the diameter of the orifice. The net rate of flow between two chambers is

$$(\pi r_o^2 v)\left[y(j+1,\theta) - y(j,\theta)\right] = (\pi r_o^2 v)\Delta y(j,\theta) \quad .$$

The difference - differential equation for the effusion of gas through a series of connecting chambers accompanied by adsorption on the chamber walls is

$$(\pi r_o^2 v)\left[\Delta y(j+1,\theta) - \Delta y(j,\theta)\right] = \frac{V_p}{NJ}(1 + c/r)\frac{d}{d\theta}y(j,\theta) \quad ,$$

$$\Delta^2 y(j,\theta) = \frac{V_p(1 + c/r)}{\pi r_o^2 vNJ}\frac{d}{d\theta}y(j,\theta) \quad .$$

If chamber J is either a dead end chamber or the center chamber of a row open at each end then

$$\Delta y(J,\theta) = 0 \quad .$$

Also

$$y(j,0) = y_o$$

$$y(0,\theta) = \bar{y}(\theta) \quad .$$

The material balance given by Equations (10) and (11) still applies if the average micropore concentration is defined

$$y(\theta) = \frac{1}{J}\sum_{j=1}^{j=J} y(j,\theta) \quad .$$

The boundary value problem can now be stated

$$\left.\begin{aligned} \Delta^2 Y(j,t') &= \frac{d}{dt'}Y(j,t') \\ Y(j,0) &= 0 \\ \Delta Y(J,t') &= 0 \\ Y(0,t') &= 1 - BY(t') \quad , \end{aligned}\right\} \qquad (48)$$

where

$$t' = \frac{\pi r_0^2 vNJ\theta}{V_p(1 + c/r)}$$

$$Y(j,t') = \left[\frac{y(j,t') - y_0}{\bar{y}_1 - y_0} \right] .$$

It is often convenient to approximate a continuous derivative by finite increments; e.g.,

$$\frac{d}{dz} V(z) \doteq \frac{\Delta V}{\Delta z} .$$

If z is of unit length and is subdivided into J increments then

$$\Delta z = \frac{1}{J} ,$$

and

$$\frac{1}{J} \frac{d}{dz} V(z) \doteq \Delta V .$$

Using the approximate operation

$$\Delta \doteq \frac{1}{J} \frac{d}{dz} ,$$

Boundary Value Problem 48 becomes

$$\left.\begin{aligned} \frac{\partial^2}{\partial z^2} Y(z,t) &= \frac{\partial}{\partial t} Y(z,t) \\ Y(z,0) &= 0 \\ \frac{\partial}{\partial z} Y(1,t) &= 0 \\ Y(0,t) &= 1 - BY(t) \end{aligned}\right\} \qquad (49)$$

where

$$t = t'/J^2 = \frac{\pi r_0^2 vN\theta}{JV_p(1 + c/r)} ; \qquad (27)$$

Since Boundary Value Problems 44 and 49 are identical, the solutions to the former are applicable to the latter providing the value for t from Equation (27) is substituted for the value from Equation (17).

APPENDIX V

NOTES ON EQUIPMENT

TABLE 18

SOURCES OF EQUIPMENT AND MATERIALS

Item	Type	Source (Company)
Agitator	1/4 HP, portable	Patterson Foundry and Machine
Autotransformer	V-20HM	General Radio
Cathetometer	72730	Central Scientific
Electrical Connectors	406-101	American Instrument
Fittings		
Ermeto	8000 Series	Weatherhead
Superpressure	406-101	American Instrument
Galvanometer	34022HH	Rubicon
Gaskets		
Electrical Connectors	3/8" extruded Teflon rod	DuPont
Heating Jacket	5"-4Y-Series 30	Goetze Gasket and Packing
Level Adjuster	D-110	Durametallic
Heating Jacket		
Calrod Heater	4A294G2	General Electric
Blind Flange	5"-300 lb.	Taylor Forge
Slip-On Flange	5"-300 lb.	Taylor Forge
Welding Cap	5"-St'd Wall	Taylor Forge
Insulation	Foamglas	Pittsburgh Corning
Lamps, Fluorescent	F42T6/W	General Electric

Item	Type	Source (Company)
Potentiometer	K	[illegible] Northrup
Pressure		
Dead Weight Tester	1000 lb.	Amthor Testing Instrument
Gages	1010T, 1012T, 105[illegible]T, 1[illegible]7	Manning, Maxwell and Moore
Regulator	[illegible]	Grove Regulator
Relay Racks	Std Heavy Duty	Communication Equipment
Safety Head	5/8T-1/4"-1/4"-[illegible]45 lb.	Black, Sivalls and Bryson
Thermometer, Precision	9 [illegible]151	Brooklyn Thermometer
Thermoregulator		
Kovar-glass Seal	96.1004	Stupakoff
Kovar Tubing	90250010	Stupakoff
Tubing		
Aluminum	50[illegible]-0, 20 [illegible] ure	Aluminum
Superpressure	1/4"o.d.x[illegible]/20"i.d.	American Instrument
Vacuum		
Diffusion Pump	[illegible]	Distillation Products
Diffusion Pump Oil	[illegible]	Central Scientific
Fore Pump	[illegible]	Welch
McLeod Gage	[illegible]156	Central Scientific
Valves	[illegible]3, 351, 460, 461, 46[illegible], 10[illegible]	Hoke

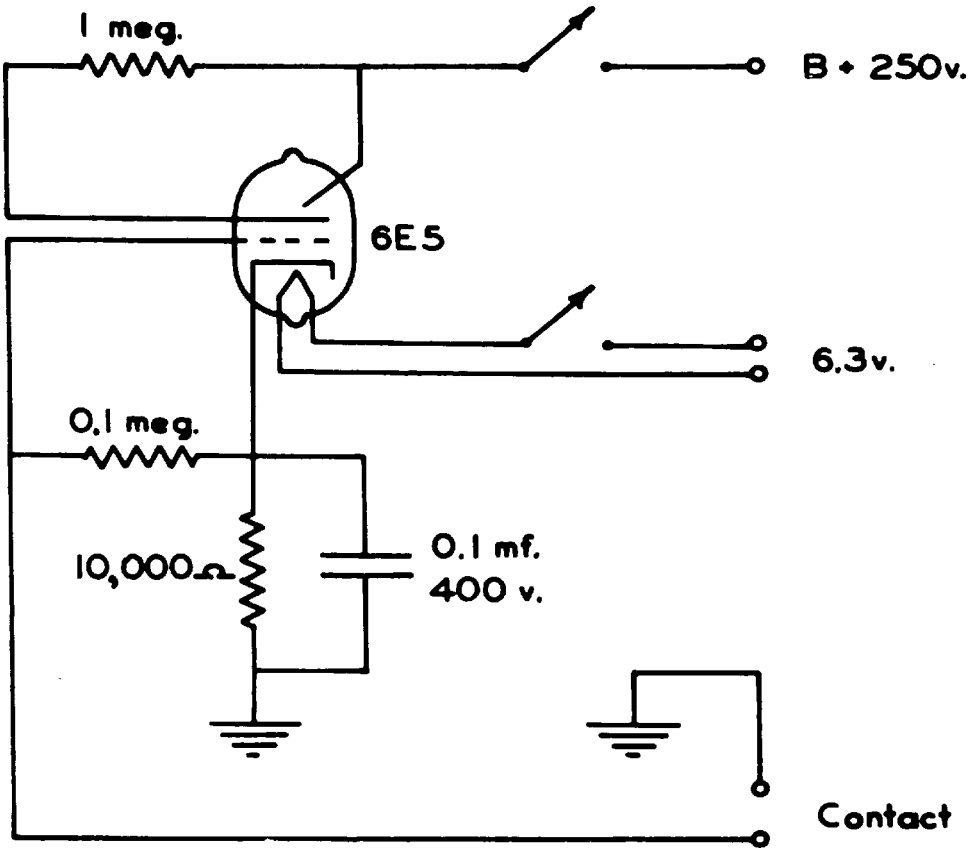

FIG. 16 TUNING EYE CONTACT INDICATOR

BIBLIOGRAPHY

BIBLIOGRAPHY

1. Advances in Catalysis and Related Subjects, edited by Frankenburg, W.G., Komarewsky, V.I., and Rideal, E.K. Academic Press, New York, Ref. (1A): Vol. I (1948); Ref. (1B): Vol. II (1950); Ref. (1C): Vol. III (1951).

2. Akers, W.W., and White, R.R. "Kinetics of Methane Synthesis," Chemical Engineering Progress, 44, 553 (1948).

3. Barr, W.E., and Anhorn, V.J. Scientific and Industrial Glass Blowing and Laboratory Techniques, Instruments Publishing Company, Pittsburgh, Pa. (1949), chapt. XII.

4. Barrer, R.M., "Fluid Flow in Porous Media," Discussions of the Faraday Society, No. 3, 61 (1948).

5. Barrer, R.M. Diffusion in and Through Solids. The Mac-Millan Company, New York (1941).

6. Barrer, R.M., and Grove, D.M. "Flow of Gases and Vapours in a Porous Medium and its Bearing on Adsorption Problems. Part II. Transient Flow," Transactions of the Faraday Society, 47, 826 (1951).

7. Barrett, E.P., Joyner, L.G., and Halenda, P.P. "The Determination of Pore Volume and Area Distributions in Porous Substances. I. Computations from Nitrogen Isotherms," Journal of the American Chemical Society, 73, 373 (1951).

8. Bergter, F. "Der zeitliche Verlauf der Absorption von Gasen durch Holzkohle," Annalen der Physik, (4) 37, 472 (1912).

9. Binder, G.G., and White, R.R. "Synthesis of Methane from Carbon Dioxide and Hydrogen," Chemical Engineering Progress, 46, 563 (1950).

10. Brunauer, S. The Adsorption of Gases and Vapors, Vol. I, Princeton University Press, Princeton (1945).

11. Carman, P.C., Malherbe, P. le R. "Diffusion and Flow of Gases and Vapors Through Micropores. II. Surface Flow," Proceedings of the Royal Society (London), A203, 165 (1950).

12. Carslaw, H.S., and Jaeger, J.C. Conduction of Heat in Solids, Clarendon Press, Oxford (1947).

13. Chemical Engineers' Handbook, edited by Perry, J.H. McGraw-Hill Book Company, New York (1950), p. 205.

14. Churchill, R.V. Modern Operational Mathematics in Engineering, McGraw-Hill Book Company, New York (1944).

15. Dushman, S. Scientific Foundations of Vacuum Technique, John Wiley and Sons, New York (1949), p. 560.

16. Hatta, Sirozi. "On the Extraction Velocity of Solids, I," Journal of the Society of Chemistry and Industry, Japan, Supplemental Binding, 39, 486 B (1936).

17. Hougen, O.A., and Watson, K.M. Chemical Process Principles, Part III, John Wiley and Sons, New York (1947).

18. Jones, W. Mervyn. "Mobility in a Sorbed Layer. Part I. The Flow of Gases and Vapours Through Porous Media," Transactions of the Faraday Society, 47, 381 (1951).

19. Joyner, L.G., Barrett, E.P., and Skold, R. "The Determination of Pore Volume and Area Distributions in Porous Substances. II. Comparison Between Nitrogen Isotherm and Mercury Porosimeter Methods," Journal of the American Chemical Society, 73, 3155 (1951).

20. Kennard, E.H. Kinetic Theory of Gases, McGraw-Hill Book Company, New York (1938).

21. Langmuir, I. "The Adsorption of Gases on Plane Surfaces of Glass, Mica and Platinum," Journal of the American Chemical Society, 40, 1361 (1918).

22. Langmuir, I. "Vapor Pressures, Evaporation, Condensation and Adsorption," Journal of the American Chemical Society, 54, 2798 (1932).

23. Latour, L.A. Harshaw Chemical Company, Private Communication (August 7, 1950).

24. Liebhafsky, H.A. "Diffusion Calculations," Journal of Applied Physics, 12, 707 (1941).

25. Matheson Company, Joliet, Ill. Data Sheets on Compressed Gases and Gas Regulators, (August, 1948).

26. Piret, E.L., Ebel, R.A., Kiang, C.T., and Armstrong, W.P. "Diffusion Rates in Extraction of Porous Solids, 1. Single Phase Extractions," Chemical Engineering Progress, 47, 405 (1951).

27. Potter, C., and Baron, S. "Kinetics of the Catalytic Formation of Phosgene," Chemical Engineering Progress, 47, 473 (1951).

28. Pursley, J.A. "An Investigation of the Reaction Between Carbon Monoxide and Hydrogen on a Nickel Catalyst at Pressures Above One Atmosphere," Ph.D. thesis in Chemical Engineering, University of Michigan (1951).

29. Ritter, H.L. and Drake, L.C. "Macropore-Size Distribution in Some Typical Porous Substances," Industrial and Engineering Chemistry, Analytical Edition, 17, 787 (1945).

30. Schwartz, C.M., and Lavender, R. "A Stable Pirani-Gauge Circuit for Indication and Control of Vacuum Equipment," Review of Scientific Instruments, 19, 814 (1948).

31. Snyder, E., and Seltz, H. "Low-Lag Toluene Thermoregulator," Industrial and Engineering Chemistry, Analytical Edition, 17, 126 (1945).

32. Sucher, I., Anker, H.S. "A Vacuum Tube Relay for Thermostat Control," Review of Scientific Instruments, 20, 321 (1949).

33. Thiele, E.W. "Relation Between Catalytic Activity and Size of Particle," Industrial and Engineering Chemistry, 31, 916 (1939).

34. Wicke, E. "Empirische und theoretische Untersuchungen der Sorptionsgeschwindigkeit von Gasen an poroesen Stoffen I," Kolloid Zeitschrift, 86, 167 (1939).

35. Wiebe, R., Gaddy, V.L., and Heins, Conrad, Jr. "The Compressibility Isotherms of Helium at Temperatures from -70 to 200° and at Pressures to 1000 Atmospheres," Journal of the American Chemical Society, 53, 1721 (1931).

36. Wild, William. "The Compressibilities of the Permanent Gases," Philosophical Magazine (7), 12, 41 (1931).

NOMENCLATURE

NOMENCLATURE

A	=	total catalyst surface area
c	=	$\Delta n'/\Delta y$, slope of adsorption isotherm
D	=	diffusivity
f	=	fraction of total catalyst surface which is readily accessible
J	=	average number of connecting microchambers in a row
k	=	adsorption rate constant
k_0	=	modified adsorption rate constant
k'	=	desorption rate constant
K	=	adsorption equilibrium constant
L	=	average length of a dead end pore or half length of an open ended pore
n	=	pV/zRT, moles of gas
n		moles of adsorbate per unit weight of catalyst
n'	=	moles of adsorbate per unit area of catalyst
n_0	=	initial value of n
n_∞	=	equilibrium value of n
n_m	=	moles of adsorbate per unit weight of catalyst to form a complete unimolecular layer
n'_m	=	moles of adsorbate per unit area of catalyst to form a complete unimolecular layer

N = total number of catalyst pores or rows of connecting microchambers

p = pressure

p_0 = initial pressure before any gas is added to (or withdrawn from) the catalyst chamber

p_0' = initial pressure after gas has been added to (or withdrawn from) the catalyst chamber assuming no adsorption (or desorption) has taken place

p_1 = initial pressure obtained by extrapolating p versus square-root of time to zero time

p_2 = initial pressure obtained by extrapolating ln $(p-p_\infty)$ versus time to zero time

p_θ = final pressure measured in any adsorption (or desorption) step

p_∞ = equilibrium pressure

r = (cross section)/(circumference), hydraulic radius

r_0 = average hydraulic radius of the orifices between a series of connecting microchambers

R = gas constant

s = transform variable

S_1 = initial slope of $p/(p_0-p_1)$ versus the square root of time

S_∞ = final slope of $\ln(p-p_\infty)$ versus time

T = temperature

v = mean molecular velocity

V_p = total catalyst pore volume or total micropore volume

$\bar{V}$ = total volume of the system less V_p

W = weight of catalyst

x = distance

y = concentration in moles per unit volume

$y(\theta)$ = average micropore concentration at time θ

$y(x,\theta)$ = micropore concentration at a distance x from micropore entrance and at time θ

$y(j,\theta)$ = concentration in the jth microchamber at time θ

y_0 = $y(0)$

y_∞ = $y(\infty)$

$\bar{y}(\theta)$ = concentration in the volume $\bar{V}$ at time θ

$\bar{y}_0$ = initial concentration in the volume $\bar{V}$ corresponding to p_0

$\bar{y}_1$ = initial concentration in the volume $\bar{V}$ corresponding to p_1

$\bar{y}_\infty$ = equilibrium concentration in the volume $\bar{V}$ corresponding to p_∞

α = condensation coefficient in the Langmuir equation

β_j = jth root of the equation $\beta_j \cot \beta_j + B = 0$

Δ = finite difference

θ = time

μ = viscosity

τ = average life of an adsorbed molecule

Dimensionless Parameters

$B = \left[V_p/\bar{V}+(1-f)E\right] /(1+fE)$, material balance constant

$E = (WRT/\bar{V})(dn/dp)$, constant in the diffusion and effusion equations

$F = WnRT/p_\infty (V_p+\bar{V})$, constant in the rate of adsorption equation

$t = D\theta/L^2 (1+c/r)$, dimensionless time factor in the diffusion equation

$t = \pi r_0^2 vN\theta/JV_p(1+c/r)$, dimensionless time factor in the effusion equation

$t' = \pi r_0^2 vNJ\theta/V_p(1+c/r)$, dimensionless time factor in the effusion equation

$Y(z,t) = \left[y(z,t)-y_0\right] /(\bar{y}_1-y_0)$, concentration ratio

$Y(t) = \left[y(t)-y_0\right] /(\bar{y}_1-y_0)$, concentration ratio

$\bar{Y}(t) = \left[\bar{y}_1-\bar{y}(t)\right] /(\bar{y}_1-y_0)$, concentration ratio

$z = pV/nRT$, compressibility factor

$z = x/L$, position ratio